Journal Pre-proof

Comprehensive molecular characterization of long-term glioblastoma survivors

Hao Xu, Xinyu Chen, Ying Sun, Xiaomu Hu, Xuan Zhang, Ye Wang, Qisheng Tang, Qiongji Zhu, Kun Song, Hong Chen, Xiaofang Sheng, Yu Yao, Dongxiao Zhuang, Lingchao Chen, Ying Mao, Zhiyong Qin

PII: S0304-3835(24)00331-8

DOI: https://doi.org/10.1016/j.canlet.2024.216938

Reference: CAN 216938

To appear in: *Cancer Letters*

Received Date: 30 January 2024

Revised Date: 1 May 2024

Accepted Date: 2 May 2024

Please cite this article as: H. Xu, X. Chen, Y. Sun, X. Hu, X. Zhang, Y. Wang, Q. Tang, Q. Zhu, K. Song, H. Chen, X. Sheng, Y. Yao, D. Zhuang, L. Chen, Y. Mao, Z. Qin, Comprehensive molecular characterization of long-term glioblastoma survivors, *Cancer Letters*, https://doi.org/10.1016/j.canlet.2024.216938.

Title: Comprehensive molecular characterization of long-term glioblastoma survivors

Hao Xu[1,2,3], Xinyu Chen[4], Ying Sun[5,6], Xiaomu Hu[7], Xuan Zhang[5], Ye Wang[1,2,3], Qisheng Tang[1,2,3], Qiongji Zhu[1,2,3], Kun Song[1,2,3], Hong Chen[7], Xiaofang Sheng[8], Yu Yao[1,2,3], Dongxiao Zhuang[1,2,3], Lingchao Chen[1,2,3], Ying Mao[1,2,3], Zhiyong Qin[1,2,3]

Hao Xu, Xinyu Chen and Ying Sun contributed equally to this work.

1.Department of Neurosurgery, Huashan Hospital, Fudan University, Shanghai, China

2.National Center for Neurological Disorders, Shanghai, China

3.Shanghai Key Laboratory of Brain Function Restoration and Neural Regeneration, Shanghai, China

4.Department of Breast and Urological Medical Oncology, Fudan University Shanghai Cancer Center, Shanghai Medical College, Fudan University, Shanghai, China

5.GenomiCare Biotechnology (Shanghai) Co. Ltd., Shanghai, China

6.Department of Data Science, Shanghai CreateCured Biotechnology Co. Ltd., Shanghai, China

7.Department of Pathology, Huashan Hospital, Fudan University, Shanghai, China

8.Department of Radiation Oncology, Huashan hospital, Fudan University, Shanghai, China

Correspondence:

Lingchao Chen, E-mail: chenlingchao12@sina.com, Phone: +86-13918577014, Fax: 86-21-62482884.

Ying Mao, E-mail: maoying@fudan.edu.cn, Phone: +86-13801769152, Fax: 86-21-52887240.

Zhiyong Qin, E-mail: qinzhiyong@fudan.edu.cn, Phone: +86-13701601840, Fax: 86-21-62482884.

Abbreviations

ATRX, ATRX chromatin remodeler; BRAF, B-Raf proto-oncogene, serine/threonine kinase; BS-Seq, bisulfite sequencing; CAPZA2, capping actin protein of muscle Z-line subunit alpha 2; CASC5, kinetochore scaffold 1; CDK1, cyclin dependent kinase 1; CGGA, Chinese Glioma Genome Atlas; CN, copy number; CNS, central nervous system; CNV, copy number variation; DEG, differentially expressed genes; DMP, differential methylated probe; EGFR, epidermal growth factor receptor; EIF4E, eukaryotic translation initiation factor 4E; FFPE, formalin-fixed, paraffin-embedded; FSIP2, fibrous sheath interacting protein 2; FZR, fizzy and cell division cycle 20 related 1; GBM, glioblastoma; GO, Gene Ontology Resource; GSEA, gene set enrichment analysis; GTR, gross total resection; H3-4, H3.4 histone, cluster member; H4C9, H4 clustered histone 9; HOXA3, homeobox A3; ICIs, immune checkpoint inhibitors, TME, tumor microenvironment; IDH, isocitrate dehydrogenase; INDEL, short insertion/deletion; INHBA, inhibin subunit beta A; KEGG, Kyoto Encyclopedia of Genes and Genomes; KIF20B, kinesin family member 20B; KMT2C, lysine methyltransferase 2C; LGG, lower grade glioma; LTS, long-term survivors; MALAT1, metastasis associated lung adenocarcinoma transcript 1; MATH score, mutant-allele tumor heterogeneity score; MET, MET proto-oncogene, receptor tyrosine kinase; MGMT, O6-methylguanine-DNA methyltransferase; MSI, microsatellite instability; MTAP, methylthioadenosine phosphorylase; NCOR2, nuclear receptor corepressor; NF1, neurofibromin 1; OS, overall survival; PCA, principal component analysis; PD-1, programmed cell death-1; PDGFRA, platelet derived growth factor receptor alpha; PIK3CA (PI3K), phosphatidylinositol-4,5-bisphosphate 3-kinase catalytic subunit alpha; PIK3R1, phosphoinositide-3-kinase regulatory subunit 1; PTCD1, pentatricopeptide repeat domain 1; PTEN, phosphatase and tensin homolog; PTPRZ1, protein tyrosine phosphatase receptor

type Z1; RB1, RB transcriptional corepressor 1; RELB, RELB proto-oncogene, NF-kB subunit; RELN, reelin; RPS6KA4, ribosomal protein S6 kinase A4; RT, radiotherapy; RTK, receptor tyrosine kinase; SHOC2, SHOC2 leucine rich repeat scaffold protein; SMC3, structural maintenance of chromosomes 3; SNV, single nucleotide variations; SPEN, spen family transcriptional repressor; SPOCD1, SPEN paralogue and orthologue C-terminal domain containing 1; ST7, suppression of tumorigenicity 7; STS, short-term survivors; TCGA, The Cancer Genome Atlas; TERT, telomerase reverse transcriptase; TMB, tumor mutation burden; TMZ, temozolomide; TP53, tumor protein p53; TSFM, Ts translation elongation factor, mitochondrial; WES, whole exome sequencing; WHO, World Health Organization

Abstract

Fewer than 5% glioblastoma (GBM) patients survive over five years and are termed long-term survivors (LTS), yet their molecular background is unclear. The present cohort included 72 isocitrate dehydrogenase (IDH)-wildtype GBM patients, consisting of 35 LTS and 37 short-term survivors (STS), and we employed whole exome sequencing, RNA-seq and DNA methylation array to delineate this largest LTS cohort to date. Although LTS and STS demonstrated analogous clinical characters and classical GBM biomarkers, *CASC5* ($P = 0.002$) and *SPEN* ($P = 0.013$) mutations were enriched in LTS, whereas gene-to-gene fusions were concentrated in STS ($P = 0.007$). Importantly, LTS exhibited higher tumor mutation burden ($P < 0.001$) and copy number (CN) increase ($P = 0.013$), but lower mutant-allele tumor heterogeneity score ($P < 0.001$) and CN decrease ($P = 0.026$). Additionally, LTS demonstrated hypermethylated genome ($P < 0.001$) relative to STS. Differentially expressed and methylated genes both enriched in olfactory transduction. Further,

analysis of the tumor microenvironment revealed higher infiltration of M1 macrophages (P = 0.043), B cells (P = 0.016), class-switched memory B cells (P = 0.002), central memory $CD4^+$ T cells (P = 0.031) and $CD4^+$ Th1 cells (P = 0.005) in LTS. We also separately analyzed a subset of patients who were methylation class-defined GBM, contributing 70.8% of the entire cohort, and obtained similar results relative to prior analyses. Finally, we demonstrated that LTS and STS could be distinguished using a subset of molecular features. Taken together, the present study delineated unique molecular attributes of LTS GBM.

Keywords

Glioblastoma, long-term survivor, mutation analysis, RNA sequencing, DNA methylation array

Introduction

Glioblastoma (GBM) is the most common primary malignant intracranial tumor in adults. Prior to 2005, patients were treated with surgical resection followed by radiotherapy and the median overall survival (OS) was approximately 12.1 months. The present standard of care, on the other hand, included maximal safe resection followed by concurrent radiotherapy and temozolomide (TMZ) chemotherapy (Stupp regimen) [1], with an OS of 14.6-16.7 months in the majority of clinical trials [1-4]. The augmentation of tumor treating fields further extended the median OS to 20.9 months [5]. Still, a high proportion of patients suffered recurrence within one year after the first surgery and only about 5% of patients survived over five years [1], hereafter termed long-term survivors (LTS) [6]. Therefore, it would be of major clinical significance to delineate the molecular characteristics of LTS GBM.

Multiple studies have confirmed that gross total resection (GTR) and completion of the Stupp regimen served to improve the OS of GBM patients [7-9]. On the other hand, lower Karnofsky performance status (KPS) score and older age were associated with unfavorable survival [10]. Some researchers also proposed patient sex as an important prognostic factor for GBM [11].

In recent years, there have been tremendous breakthroughs in unraveling the molecular features of glioma, with the most overarching discovery being the mutation of isocitrate dehydrogenase (IDH) gene associated with better prognosis, location in hemisphere instead of midline and sensitivity to chemoradiotherapy [12, 13]. However, IDH mutation is typically observed in lower grade glioma (LGG) which is different from primary IDH-wildtype GBM in terms of methylation and gene expression profile [12].

In addition to IDH mutation, O^6-methylguanine-DNA methyltransferase (*MGMT*) promoter methylation has been proved to be associated with TMZ sensitivity [14]. Telomerase reverse transcriptase (*TERT*) promoter mutation was also frequently observed in GBM and predicted aggressive clinical behavior [15]. Multiple studies have identified epidermal growth factor receptor (*EGFR*) amplification to be associated with significantly shorter survival [15]. Similarly, the signature of whole chromosome 7 gain and whole chromosome 10 loss (+7/−10) demonstrated high specificity for predicting aggressive behavior and poor prognosis in IDH-wildtype astrocytic gliomas [16]. Some studies have reported higher expression of RELB proto-oncogene, NF-kB subunit (*RELB)* to be associated with shorter survival in GBM [17]. Although ATRX chromatin remodeler (*ATRX*) mutations were frequently observed in IDH-mutant astrocytoma and associated with improved survival, they were rare in IDH-wildtype astrocytoma [18, 19].

Several studies attempted to characterize LTS and establish clinically relevant biomarkers [20, 21]. One study focusing on LTS GBM with alteration in receptor tyrosine kinase/phosphatidylinositol-4,5-bisphosphate 3-kinase (RTK/PI3K), tumor protein p53 (*TP53*) or RB transcriptional corepressor 1 (*RB1*) pathway identified platelet derived growth factor receptor alpha (*PDGFRA*) alteration as a favorable prognostic factor [22]. In addition, CD34 expression served as a candidate in GBM to distinguish survival outliers [20]. Notably, one recent study based on multi-omics revealed that DNA repair and cell cycle pathways were enriched in short-term survivors (STS). In contrast, the sphingomyelin metabolism pathway was enriched in LTS [21]. Despite the above biomarker candidates, integrative molecular analysis to distinguish LTS from the general GBM cohort remains sparse. Furthermore, most previous studies regarded GBM as a single entity irrespective of IDH mutation status.

In the present study, we adopted the largest set of LTS GBM to date (n = 35) based on the 2021 World Health Organization Classification of Tumors of the Central Nervous System (WHO CNS5), and conducted integrative genomic, transcriptomic, and epigenetic analyses to better understand the molecular profile of LTS GBM patients [23].

Materials and Methods

Patient recruitment

This single-institution study was approved by the Ethics Committee of Huashan Hospital, Fudan University Shanghai, China 200040 (No.KY2015-256). Primary GBM patients who underwent the first surgery at the Department of Neurosurgery, Huashan Hospital between October 2010 and September 2017 were retrospectively analyzed, and recurrent cases were excluded from the present

study. Informed consent was signed by each patient preoperatively and all patients agreed to donate their remnant tumor tissue, blood sample and the associated clinical information to Huashan Hospital Standardized Glioma Tissue Bank (GTB) on the premise that the diagnostic procedure and clinical treatment were not compromised by the collection process [24].

OS was defined from the date of surgery to the date of death due to any cause. Patients meeting the following criteria were eligible for the LTS group: (1) OS exceeding five years; (2) age 18 or older; (3) histologically diagnosed as GBM and confirmed as IDH-wildtype; (4) tumor available for analysis; and (5) without preoperative TMZ administration.

Of all 2034 patients, 109 exceeded the 5-year OS. Among these patients, 92 possessed sufficient tissue for multi-omics analysis evaluated by an experienced neuropathologist, including 37 IDH-wildtype and 55 IDH-mutant tumors (**Supplementary Fig. S1a**).

Patients in the STS cohort underwent surgery at Huashan Hospital between July 2018 and January 2021, and should meet all the above criteria except for criterion 1 and instead required a less than 24-month OS. Central pathology review was performed by the Department of Pathology based on 2021 WHO CNS5.

348 STS patients were initially identified. Of all 317 STS patients who possessed sufficient tissue, 305 were confirmed as IDH-wildtype and 37 cases were randomly selected as STS for analysis (**Supplementary Fig. S1a**).

The Cancer Genome Atlas (TCGA) was accessed through Genomic Data Commons (GDC) (https://portal.gdc.cancer.gov) and LTS patients were selected based on the following criteria: (1) project ID as TCGA-GBM; (2) with open access (not controlled); (3) “brain” as primary site; (4)

"primary tumor" as sample type; (5) IDH-wildtype; (6) with OS ≥ three years; (7) possessed 450K methylation array, SNV or RNA-seq count data, and (8) excluded secondary GBM.

Similarly, LTS patients from Chinese Glioma Genome Atlas (CGGA) database (www.cgga.org.cn) were selected: (1) histology being GBM; (2) IDH-wildtype; (3) with OS ≥ three years; (4) RNA-seq, DNA sequencing or DNA methylation data available, and (5) excluded secondary and recurrent GBM.

Whole exome sequencing (WES)

WES was performed at the Genomics Laboratory of GenomicCare Biotechnology (Shanghai, China). For frozen blood, DNA was extracted from thawed materials using the Maxwell RSC Blood DNA Kit (AS1400, Promega, Madison, WI, USA) on a Maxwell RSC system (AS4500, Promega). For formalin-fixed, paraffin-embedded (FFPE) tissue, DNA was extracted using the MagMAX FFPE DNA/RNA Ultra Kit (A31881, ThermoFisher, Waltham, MA, USA) on a KingFisher Flex system (ThermoFisher). The extracted DNA was sheared using a Covaris L220 sonicator, captured using the SureSelect Human All Exon V7 kit (5991-9039EN, Agilent, Santa Clara, CA USA), prepared to library using the SureSelectXT Low Input Target Enrichment and Library Preparation System (G9703-90000, Agilent), and sequenced using the Illumina NovaSeq-6000 System (Illumina, San Diego, CA, USA) to generate 2x150 bp paired end reads. Image analysis and base calling was performed using onboard RTA3 software (Illumina).

Data quality control

The quality of data was checked by monitoring the coverage and depths of sequence. RNA-seq was performed with an average depth over 150x, while WES reached an average depth over 180x for tumor samples and over 49x for normal samples (**Supplementary Table 1**). After removing adapters and low-quality reads (base quality < 20), all reads were aligned to NCBI human genome reference assembly GRCh37/hg19 using the Burrows-Wheeler Aligner algorithm [25].

Somatic variant identification

The Sentieon (version 201911) running environment was implemented to process the following steps with default parameters: read alignment to GRCh37/hg19, duplication sorting, realignment and recalibration, and somatic mutation calling including single nucleotide variation (SNV) and short insertion/deletion (INDEL) [26]. During the mutation calling stage, the reads from the tumor sample were compared to the blood sample from the same patient. The called somatic mutations were then filtered, retaining only mutations with variant allele frequency ≥ 0.05 and supported by at least three reads, and annotated using the Variant Effect Predictor package [27]. Mutant-allele tumor heterogeneity (MATH) score was calculated using the math.score package [28]. The mutually exclusive and co-occurring gene mutations were calculated and visualized by the maftools package in R [29].

Tumor mutation burden (TMB)

TMB score in counts/Mb was defined as the total number of somatic nonsynonymous mutations (SNV or INDEL) in the tumor exome divided by the size of the targeted region. The SureSelect

Human All Exon V7 Kit (Agilent) was used for the present study and its estimated total targeting size (exome) was 35 Mb.

Copy number variation (CNV)

The normalized depth-of-coverage ratio approach was used to identify CNV based on WES analysis of paired samples using the ExomeCNV package [30]. Standard normal distribution was used to offset five sources of bias including exon size, batch effect, quantity and quality of the sequencing data, local GC content, and genomic mappability. Genes with haploid CN $\leq$ 1, 1 < CN $\leq$ 1.2, 3 $\leq$ CN < 4 and CN $\geq$ 4 were defined as deletion, loss, gain and amplification, respectively, and a minimum tumor content (purity) of 20% was required.

Microsatellite instability (MSI)

All autosomal microsatellite tracts containing five or more repeating subunits 1-5 bp in length based on GRCh37/hg19 were identified using MISA (http://pgrc.ipk-gater sleben.de/misa/misa.html). MSIsensor was used for MSI calling and patients with $\geq$ 3.5% unstable microsatellite sites were defined as MSI-high [31].

Mutational signature analysis

The COSMIC database (https://cancer.sanger.ac.uk/cosmic/signatures) was used to calculate the cosine similarity between tumor mutational profile and 30 known COSMIC signatures. The results were clustered with the seaborn package (https://joss.theoj.org/papers/10.21105/joss.03021) and

tsne analysis was performed with the sklearn package (https://scikit-learn.org/stable/index.html), and matplotlib in Python (https://matplotlib.org/stable/index.html) was adopted for visualization.

RNA-seq data analysis

RNA from FFPE was purified using the MagMAX FFPE DNA/RNA Ultra Kit (A31881, ThermoFisher) on a KingFisher Flex system (ThermoFisher) and used as the template to synthesize cDNA using NEBNext RNA First Strand Synthesis Module (E7525S, NEB, Waltham, MA, USA) and NEBNext mRNA Second Strand Synthesis Module (E6111S, NEB) sequentially.

Library preparation and sequencing were performed the same as in WES. RNA-seq reads were assembled using StringTie2 (version 1.3.5), and an expression matrix including fragments per kilobase of exon model per million mapped fragments and transcripts per kilobase of exon model per million mapped reads was generated [32]. RNA-seq reads were mapped to GRCh37/hg19 using STAR (version 020201) [33], and the raw read counts were further normalized by log2-counts per million normalization. A list of differentially expressed genes (DEGs) between LTS and STS were calculated using DESeq2 with the following criteria: FDR value <0.05, absolute value of log2 fold change > 2 [34]. Biological pathway enrichment was performed using the Kyoto Encyclopedia of Genes and Genomes (KEGG) [35] and the Gene Ontology Resource (GO) [36].

Immune cell infiltration analysis

RNA-seq transcripts per million data was used to calculate the immunopheno score using the R package XCELL [37]. Infiltrating cell types were clustered and visualized by the R package ComplexHeatmap [38] and ggplot2 [39].

GISTIC analysis

GISTIC analysis was performed using Gistic2.0 with the following parameters: -rx 0 -genegistic 1 -smallmem 1 -broad 1 -brlen 0.7 -twosize 1 -armpeel 1 -savegene 1 -maxseg 10000 -conf 0.99 -ta 0.1 -td 0.1 -js 50 [40].

Gene fusion analysis

Transcripts were assigned using StringTie2 (version 1.3.5) [32], and fusion genes were identified using STAR-FUSION (version 1.8.0) [41] requiring at least three supporting reads during fusion gene calling [41]. In addition, genes annotated as "probably false positive" by FusionHub (https://fusionhub.persistent.co.in/) were excluded.

Clustering and principal component analysis (PCA) of expression data

The R package ConsensusClusterPlus was used for clustering with the parameters: maxK = 7, reps = 500, pItem = 0.6, pFeature = 1, clusterAlg = "pam", seed = 10 [42]. As for heatmap display, genes were ranked by standard deviation across all samples in descending order and the top 2000 genes were used for clustering through the pheatmap package [43]. PCA was performed using the prcomp function in R to project samples into a two-dimensional space, and the first two PCs were used for plotting.

Bisulfite sequencing (BS-seq) and methylation-based classification

Illumina Infinium Methylation EPIC BeadChip was used for bisulfite sequencing ChIP assay. DNA was extracted and all procedures were conducted according to the Infinium HD Methylation Assay Reference Guide (15019519 v07, Illumina) to generate raw data files. The R package ChAMP was used to process raw data and probes with absolute deltaBeta > 0.1 and FDR < 0.05 were considered differentially methylated probes (DMPs) [44]. HyperDMPs were defined as probes with higher average beta-value in LTS compared to STS, and hypoDMPs were defined vice versa. The methylated CpG sites were divided into three types: island shore (1 to 2,000 bp from island), island shelve (2,001 to 4,000 bp from island) and open sea (> 4,000 bp from island) [45]. DNA methylation-based classification was conducted using brain tumor classifier 12.8 (https://www.molecularneuropathology.org/.

***MGMT* promoter methylation**

The mean methylation percentages of the 1st to 12th CpG islands were calculated, and the result was considered positive if > 10%.

Immunohistochemistry (IHC)

All patient specimens were immunostained according to the manufacturers' protocol using the following primary antibodies: IFN-γ (1:50, 15365-1-AP, Proteintech), iNOS (1:50, 22226-1-AP, Proteintech), CD19 (1:25, 27949-1-AP, Proteintech), CD70 (1:50, 67749-1-Ig, Proteintech) and CD80 (1:50, 66406-1-Ig, Proteintech). Scanning was performed with a Vectra automated multispectral microscope (Olympus BX53), and the inForm software (PerkinElmer) was used for analysis.

LASSO regression

LASSO regression was performed through the package sklearn [46]. In brief, the input data included six clinical features (tumor location, gender, age, extent of resection, KPS score and completion of Stupp regimen), SNV (taking into account mutations observed in at least five patients), DEGs and DMPs. 70% of all patients were selected at random as the training set and the remaining 30% were used as the validation set. The LogisticRegression function was used with the following parameters: penalty = “elasticnet”, solver = “saga”, multi_class = “multinomial”, l1_ratio = 1, max_iter = 200, random_state = None, tol = 1e-5, and C, which was searched in the range np.logspace(-3, 2, num = 100) (https://realpython.com/logistic-regression-python/). The optimum C value was determined through minimizing the number of remaining features while maximizing the prediction precision.

Statistics and reproducibility

The R packages ggplot2, pheatmap, DESeq2 and maftools, and the Python packages seaborn and matplotlib were used for plotting, unless specifically mentioned. For P value calculation, the Pearson’s Chi-square test was used for categorical variables and the two-sided Mann Whitney U test was used for continuous variables. Survival was estimated by the Kaplan-Meier method and the Log-rank test was used to assess the statistical significance among different cohorts. Gene set enrichment analysis (GSEA) was performed using the GSEA software (http://software.broadinstitute.org/gsea/index.jsp).

Results

Cohort description

A total of 74 patients were initially included in the present study, with 37 in STS and 37 in LTS. A flow chart of the study design is presented in **Fig. 1a**. Through DNA methylation-based classification, two LTS patients were identified as pleomorphic xanthoastrocytoma with B-Raf proto-oncogene, serine/threonine kinase (*BRAF*) *V600E* mutation (**Fig. 1b, Supplementary Fig. S1b, Table 1**), and were removed from LTS cohort. The remaining 72-patient cohort is hereafter referred to as cGBM since it consisted entirely of Chinese patients, and its clinical and molecular features were summarized in **Fig. 1c**.

Clinicopathological characteristics of the two groups are listed in **Table 2**. No difference in gender (P = 0.459), age (median STS 53 years versus LTS 55 years, P > 0.999) or tumor location (P = 0.884) was found, and the KPS scores of LTS (81.7 ± 13.4) and STS (78.6 ± 15.7) (P = 0.376) were similar (**Supplementary Table 2**). Importantly, LTS and STS were comparable in terms of the treatment received, with a GTR rate of 71% in LTS and 65% in STS (P = 0.358) and a Stupp regimen acceptance rate of 83% in LTS and 81% in STS (P = 0.186). Both groups received a median of six cycles of TMZ (**Supplementary Table 2**). Additionally, LTS and STS received similar salvage therapies (P > 0.05) (**Supplementary Table 3**). The incidences of *TERT* promoter mutations (P = 0.797), *MGMT* promoter methylation (P = 0.351), +7/–10 signature (P > 0.999), and *EGFR* amplification (P = 0.817) were also similar.

Molecular landscape of the cGBM cohort

Molecular characteristics of the cGBM cohort including SNV, MATH score, gene fusion, CNV, DNA methylation and distribution of 30 COSMIC signatures are summarized in **Fig. 1c** and

Supplementary Table 2. *TP53* (36%), phosphatase and tensin homolog (*PTEN*) (28%), neurofibromin 1 (*NF1*) (25%), lysine methyltransferase 2C (*KMT2C*) (22%) and *EGFR* (21%) demonstrated the highest mutation rate in cGBM (**Supplementary Fig. S1c**). In LTS, *TP53* (40%), *KMT2C* (34%), *NF1* (31%) and *PTEN* (29%) were the top 4 highly mutated genes, whereas *TP53* (32%), *PTEN* (27%), *EGFR* (24%) and *NF1* (19%) demonstrated the highest mutation rate in STS (**Supplementary Fig. S1d**). For classical GBM molecular biomarkers such as *PTEN* ($P > 0.999$), *TP53* ($P = 0.625$) and *EGFR* ($P = 0.566$) mutations, no difference was observed between LTS and STS (**Supplementary Fig. S1d**).

As for CNVs, *EGFR* (44%), homeobox A3 (*HOXA3*) (39%), H3.4 histone, cluster member (*H3-4*) (33%) showed the highest rate of CN increase (CN gain and CN amplification), while cyclin dependent kinase 1 (*CDK1*) (31%) and kinesin family member 20B (*KIF20B*) (28%) demonstrated the highest rate of CN decrease (CN loss and CN deletion) in cGBM (**Supplementary Fig. S1e**). In LTS, *H3-4* (46%), *HOXA3* (43%) and *EGFR* (43%) demonstrated the highest rate of CN increase, while metastasis associated lung adenocarcinoma transcript 1 (*MALAT1*) (29%) and methylthioadenosine phosphorylase (*MTAP*) (11%) demonstrated the most frequent CN decreases. Considering STS counterparts, *EGFR* (46%), *HOXA3* (35%) and *H3-4* (22%) also demonstrated the top CN increases and *KIF20B* (51%), *CDK1* (49%) showed the most frequent CN decreases. Comparing genes with CN increases in both groups, no difference was observed for *HOXA3* ($P = 0.630$) and *EGFR* ($P = 0.817$), while CN increases of *H3-4* ($P = 0.045$) were accumulated in LTS. Meanwhile, CN decreases of *MALAT1* ($P = 0.011$) was predominant in LTS and those of *MTAP* ($P = 0.007$), *KIF20B* ($P < 0.001$) and *CDK1* ($P = 0.001$) were enriched in STS (**Supplementary Fig. S1f**). In addition, gene fusion was rarely observed in cGBM (**Supplementary Fig. S1g**).

We also compared the somatic mutation spectrum of cGBM with the TCGA GBM cohort (TCGA-GBM) (**Supplementary Table 4**). Both groups shared similar highly mutated genes including *PTEN* (P = 0.252), *TP53* (P = 0.469), *EGFR* (P = 0.871), *RB1* (P = 0.127), phosphoinositide-3-kinase regulatory subunit 1 (*PIK3R1*) (P = 0.658), *ATRX* (P > 0.999) and phosphatidylinositol-4,5-bisphosphate 3-kinase catalytic subunit alpha (*PIK3CA*) (P = 0.372). However, cGBM demonstrated higher mutation rate considering spen family transcriptional repressor (*SPEN*) (P = 0.019), *KMT2C* (P < 0.001), reelin (*RELN*) (P = 0.007) and *NF1* (P = 0.014) (**Supplementary Fig. S1h**).

In addition, we analyzed the contribution of COSMIC signatures. COSMIC signature 1, related to deamination of 5-methylcytosine, was a common signature in both LTS and STS, suggesting the importance of epigenetic regulation (**Fig. 1d-e**). The three signatures extracted from LTS patients' single nucleotide variation spectrum showed cosine similarities of 96.1%, 84.6% and 82.1% to COSMIC signatures 11, 6 and 1, respectively (**Fig. 1d**), while those extracted from STS demonstrated similarities of 92.4%, 81.1% and 21.3% to COSMIC signatures 1, 5 and 3 (**Fig. 1e**). COSMIC signatures 11 (exposure to alkylating agents) and 6 (defective DNA mismatch repair) were enriched exclusively in LTS.

Genomic alteration landscape between LTS and STS

Somatic mutation, gene fusion and CNV were compared between LTS and STS. Although LTS exhibited significantly higher TMB (**Fig. 2a**, P < 0.001), STS possessed stronger heterogeneity as indicated by higher MATH score (**Fig. 2b**, P < 0.001). Additionally, we observed more frequent gene fusions in STS (P = 0.007) (**Fig. 2c**). As for CNV, LTS exhibited more CN increases (P =

0.013) but fewer CN decreases (P = 0.026), while the difference between LTS and STS did not reach statistical significance considering the general CNV events (P = 0.141) (**Fig. 2d-e**).

Specifically, kinetochore scaffold 1 (*CASC5*) (STS 0, LTS 8, P = 0.002), *SPEN* (STS 1, LTS 8, P = 0.013) and nuclear receptor corepressor (*NCOR2*) (STS 0, LTS 5, P = 0.023) mutations were enriched in LTS (**Fig. 2f**, **Supplementary Fig. S2a**). In CASC5 protein, a hot spot mutation E110K was predicted as non-synonymous, while no hot spot was observed in SPEN (**Supplementary Fig. S2b-c**).

MET proto-oncogene, receptor tyrosine kinase (*MET*) gene fusions were exclusively observed in STS (STS 5, LTS 0, P = 0.054), including capping actin protein of muscle Z-line subunit alpha 2 (*CAPZA2*)-*MET*, suppression of tumorigenicity 7 (*ST7*)-*MET*, *MET*-Ts translation elongation factor, mitochondrial (*TSFM*), and protein tyrosine phosphatase receptor type Z1 (*PTPRZ1*)-*MET* (**Fig. 2f**, **Supplementary Fig. S1g**).

CN increases of ribosomal protein S6 kinase A4 (*RPS6KA4*) (STS 2, LTS 13, P = 0.001), fizzy and cell division cycle 20 related 1 (*FZR*) (STS 0 LTS 8, P = 0.002) and pentatricopeptide repeat domain 1 (*PTCD1*) (STS 0, LTS 8, P = 0.002) were enriched in LTS, whereas CN decreases of *KIF20B* (STS 19, LTS 1, P < 0.001), *PTEN* (STS 15, LTS 1, P < 0.001), SHOC2 leucine rich repeat scaffold protein (*SHOC2*) (STS 12, LTS 0, P < 0.001), *CKD1* (STS 18, LTS 4, P < 0.001) and structural maintenance of chromosomes 3 (*SMC3*) (STS 10, LTS 0, P = 0.001) were predominant in STS (**Fig. 2f**, **Supplementary Fig. S2d**).

RNA sequencing and tumor microenvironment analysis

We performed RNA-seq on 68 out of 72 patients and identified 18629 distinct coding genes. The top 5000 genes with highest standard deviation among all samples were clustered but failed to distinguish LTS from STS (**Supplementary Fig. S3a**). We further analyzed the 14 left most LTS patients in **Supplementary Fig. S3a** who exhibited higher expression of gene cluster 2 (n = 882) relative to all other patients. Since these 882 genes may prove a marker for good prognosis, we termed it cluster R2 and the 14 patients as cluster R2 patients.

There were 3 down-regulated and 2095 up-regulated DEGs in LTS relative to STS with statistical significance (**Fig. 3a**). GO analysis of all DEGs revealed the olfactory transduction pathway to be most significantly enriched with an overlap of 79% genes in the set ($P < 0.001$, **Fig. 3b**). This was further confirmed through KEGG analysis ($P < 0.001$, **Supplementary Fig. S3b**), providing molecular-level evidence underlying olfactory transduction and GBM prognosis.

Immune checkpoint inhibitors (ICIs) draw increasing interest and tumor microenvironment (TME) may be one of the most important factors determining response to ICIs. We found lymphoid progenitor cells, T cells, NK cells, endothelial cells and hematopoietic stem cells as the predominant infiltrating cells of the entire cohort (**Fig. 3c**). Compared to STS, LTS exhibited higher infiltration of M1 macrophages ($P = 0.043$), B cells ($P = 0.016$), class-switched memory B cells ($P = 0.002$), central memory $CD4^+$ T cells ($P = 0.031$) and $CD4^+$ Th1 cells ($P = 0.005$). $CD4^+$ Th2 cells ($P = 0.013$) and plasma B cells ($P < 0.001$), meanwhile, demonstrated higher infiltration in STS (**Fig. 3d**, **Supplementary Fig. S4**). We further performed IHC and found the protein levels of IFN-γ ($P < 0.001$), iNOS ($P = 0.004$), CD19 ($P < 0.001$), CD70 ($P = 0.026$) and CD80 ($P = 0.019$) (**Fig. 3e**) were significantly higher in LTS, supporting higher infiltration of M1 macrophages, $CD4^+$ Th1 cells and activated antitumor lymphocytes.

DNA methylation pattern

The average beta value of LTS was significantly higher than that of STS regardless of CpG gene locus or CpG type (**Fig. 4a**, **Supplementary Fig. S5a**). A total of 5747 DMPs were identified comprising of 1964 hyperDMPs and 3783 hypoDMPs (**Fig. 4b**). The detailed DMP distribution is shown in **Supplementary Fig. S5b**. For CpG island, there were 409 hyperDMPs but only 33 hypoDMPs. In accordance with previous transcriptomic analysis, GSEA of DMPs also revealed enrichment of the olfactory transduction pathway, suggesting relevance between survival and epigenetic regulation of the olfaction (**Fig. 4c**). Further, PCA of DMPs demonstrated a trend of separation (**Supplementary Fig. S5c**, **Supplementary Table 5**).

Although normalized beta values of all 5747 DMPs between LTS and STS showed mixed clustering, a small group of hypermethylated probes (cluster M2) were enriched predominantly among LTS (**Supplementary Fig. S5d**), and it showed poor overlapping with cluster R2 (**Fig. 4d**). Among the 35 LTS patients with either RNA expression or methylation data, 20 (57%) could be marked by either cluster M2 or R2 (**Fig. 4d**). Therefore, the combination of clusters R2 and M2 demonstrated the potential to be LTS GBM markers.

Through methylation-based classification, only five LTS and one STS demonstrated calibrated classifier score < 0.9 and failed to match an established class [47]. In LTS group, we identified three LTS samples as inflammatory microenvironment, one as CNS tumor with *BCOR-BCORL1* fusion, and 24 were CNS WHO grade 4 tumors (m-grade 4) (**Fig. 1b**, **Table 1**, **Supplementary Fig. S1b**). Within m-grade 4 cases, one patient was found to be adult-type diffuse high grade glioma, IDH-wildtype, subtype E (HGG_E), a provisional methylation subtype which lacked molecular and

clinical information [48], and we termed the remaining 23 patients as m-GBM. As for STS, apart from three inflammatory microenvironment samples, 33 were defined as CNS WHO grade 4 tumors including 28 m-GBMs, one HGG-F and four pediatric-type high grade gliomas (**Fig. 1b, Table 1**). Collectively, the majority of LTS and STS tumors were proven as m-GBM through DNA methylation-based classification.

Molecular profiling of m-GBM

We next analyzed somatic mutation, gene fusion and CNV in m-GBM. Although incidences of *TERT* mutation (LTS 18/23, STS 22/28, P > 0.999) and + 7/− 10 signature (LTS 14/23, STS 17/28, P > 0.999) were similar between LTS and STS m-GBM cases, LTS possessed substantially higher *MGMT* promoter methylation rate than STS (LTS 20/23, STS 16/28, P = 0.030). Interestingly, analyses of MATH score, TMB, gene fusion and CN demonstrated results analogous to previous findings in that LTS possessed higher TMB level (P < 0.001, **Fig. 5a**), whereas STS exhibited higher MATH score (P < 0.001, **Fig. 5b**), more frequent gene fusions (P = 0.002, **Fig. 5c**) and more CN decreases (P = 0.048, **Fig. 5d**). No discernible difference was identified considering CN increase (P = 0.330, **Fig. 5d**) and general CNV events (P = 0.892, **Fig. 5d**).

Among m-GBM cases, *CASC5* (STS 0, LTS 6, P = 0.006), eukaryotic translation initiation factor 4E (*EIF4E*) (STS 0, LTS 4, P = 0.035) and *KMT2C* (STS 0, LTS 4, P = 0.048) mutations were accumulated in LTS, and CN increases of *PTCD1* (STS 0, LTS 6, P = 0.006), *RPS6KA4* (STS 1, LTS 8, P = 0.007) predominantly occurred in LTS (**Fig. 5e**). As for STS, CN increases of H4 clustered histone 9 (*H4C9*) (STS 7, LTS 0, P = 0.012) and inhibin subunit beta A (*INHBA*) (STS 7, LTS 0, P = 0.012) were exclusively present, a result different from previous analysis. STS was also

characterized by *MET* gene fusions (STS 4, LTS 0, P = 0.242) and CN decreases of *KIF20B* (STS 17, LTS 1, P < 0.001), *PTEN* (STS 14, LTS 1, P < 0.001), *SHOC2* (STS 11, LTS 0, P < 0.001) and *SMC3* (STS 11, LTS 0, P = 0.001) (**Fig. 5e**). Furthermore, GO analysis of DEGs revealed olfactory transduction remained the most significantly enriched pathway (P < 0.001, **Fig. 5f**) and LTS possessed hypermethylated genome compared to STS regardless of CpG gene locus or CpG type (P < 0.001, **Fig. 5g, Supplementary Fig. S5e**). In general, these results of m-GBM patients were in accordance with the molecular features of the entire cohort.

Notably, a subset of STS (n = 4) was identified as diffuse pediatric-type high grade gliomas including three diffuse pediatric-type high grade gliomas, RTK1 subtype, subclass A (pedHGG_RTK1A) and one diffuse paediatric-type high grade glioma, H3 wildtype and IDH-wild type, Subtype A (pedHGG_A) (**Fig. 1b**). These four STS patients demonstrated significantly shorter overall survival compared to STS m-GBM cases (P = 0.038, **Fig. 5h**). The average age of these four patients was 59.5 years and they were diagnosed as GBM through histopathology (**Fig.5i**). Furthermore, these pedHGG tumors not only lacked classical GBM biomarkers such as *TERT* mutation (1/4, P = 0.057 compared to STS m-GBM cases) and +7/−10 signature (0/4, P = 0.038), but were also enriched for *PDGFRA* amplification (3/4, STS m-GBM 5/28, P = 0.039) (**Fig. 5j**). Interestingly, pedHGG also demonstrated hypomethylated genome compared to STS m-GBM (P < 0.001, **Fig. 5k**, **Supplementary Fig. S5f**).

Distinguishing LTS from STS through a subset of molecular features

Our findings indicated that relying solely on gene mutation (**Supplementary Fig. S1c**), RNA expression (**Supplementary Fig. S3a**) or DNA methylation (**Supplementary Fig. S5d**) of all genes

failed to distinguish LTS from STS. We then investigated if selecting a specific gene subset from the omics data served to depict the representative characteristics of LTS. In total, 6 clinical features, 8 glioma biomarkers, mutation of 47 genes based on WES, 2098 DEGs and 4142 DMPs were adopted for LASSO regression (**Supplementary Table 6**). Mere clinical features, well-known glioma biomarkers or SNV data led to an approximate test score of 0.550, indicating poor prediction ability (**Fig. 6a-b**, **Supplementary Fig. S6a**). Although RNA expression data could achieve relatively high prediction accuracy (test score = 0.900) with the fewest features (n = 62) (**Fig. 6c**), STS and LTS showed mixed clustering (**Supplementary Fig. S6b**). Meanwhile, DMPs could lead to satisfying performance (test score = 0.952) with 862 features (**Fig. 6d**), but STS and LTS still showed a heterogeneous clustering (**Supplementary Fig. S6c**). The multi-omics data, consisting of 328-gene expression, 785-gene methylation data and 4 clinical features (**Supplementary Table 7**), not only resulted in the best performance (test score = 1.000, n = 1117) (**Fig. 6e**), but also distinguished LTS from STS **(Fig. 6f)**. Interestingly, this set of multi-omics data was significantly enriched in olfactory transduction (**Supplementary Fig. S6d**).

Finally, we analyzed the long-term survivors using TCGA and CGGA GBM datasets (**Supplementary Table 8**). In CGGA LTS, the top 4 highly mutated genes, *TP53* (40%), *PTEN* (20%), fibrous sheath interacting protein 2 (*FSIP2*) (20%) and *NF1* (10%), significantly overlapped with those of our LTS cohort (**Supplementary Fig. S1d**, **Supplementary Fig. S6e**). Although DEGs were not enriched in olfactory transduction (**Supplementary Fig. S6f**), the DNA methylation level was also higher in LTS regardless of CpG gene locus or CpG type ($P < 0.001$, **Supplementary Fig. S6g-h**).

Discussion

As one of the most fatal and challenging diseases, GBM is associated with frequent recurrence and poor prognosis, and reports on GBM patients surviving over five years are rare. A comprehensive summary of recent studies concerning LTS GBM is presented in **Supplementary Table 9** [21, 49-60]. Most studies focused on clinical features and classical glioma biomarkers and included IDH-mutant GBM defined by WHO CNS4, albeit limited sample size. Therefore, multi-omics studies incorporating relatively large IDH-wildtype LTS GBM cohort ($n \geqslant 30$) are urgently needed.

In the present study, we adopted 35 GBM LTS, representing the largest cohort to date, similar clinical features including gender, age, tumor location, KPS score, GTR rate and chemoradiotherapy use were observed between LTS and STS, suggesting the importance of molecular background in LTS patients.

According to the current WHO CNS5, GBM is defined as a diffuse astrocytic glioma with no IDH or histone H3 gene mutation while characterized by molecular features including *TERT* promoter mutation, *EGFR* amplification and +7/–10 signature. Although *MGMT* promoter methylation, associated with TMZ sensitivity [14], was higher in methylation class-defined LTS GBM, we observed no difference in *TERT* promoter mutation, *EGFR* amplification and +7/–10 signature between LTS and STS. These findings underscored the limitation regarding known GBM biomarkers in predicting survival outliers.

In GBM, *TERT* promoter mutations were associated with worse prognosis [61]. A recent meta-analysis including 10 studies and 1074 GBM patients demonstrated that high *EGFR* expression was associated with poor prognosis [62]. The +7/−10 signature also demonstrated high specificity for predicting aggressive behavior among IDH-wildtype astrocytic gliomas [16]. The presence of *BRAF*

V600E was associated with epithelioid GBM [63] and reported to demonstrate more aggressive behavior and poorer prognosis [64]. In addition, *RELB* expression was found to be associated with shorter survival in GBM. By contrast, *ATRX* mutation were frequently observed in IDH-mutant astrocytomas and associated with better survival [65].

In the present study, mutations in *SPEN* and *CASC5* were enriched in LTS. *SPEN* is a hormone inducible transcriptional repressor and highly related to Notch pathway [66], and its paralogue and orthologue C-terminal domain containing 1 (*SPOCD1*) has been recently identified in glioma to be associated with tumor proliferation and poor prognosis [67]. CASC5 is a component of the multiprotein assembly required for kinetochore-microtubule attachment and chromosome segregation, and its mutation led to loss of protein function [68]. *CASC5* loss reduced cell proliferation and triggered cell cycle arrest and apoptosis both in vitro and vivo, serving as a potential treatment target [69]. In contrast, *MET* gene fusions were exclusively observed among STS in line with previous studies, suggesting potential association with poor prognosis and glioma progression [70].

Even within a single GBM lesion, there could be multiple subclones with distinct molecular profiles [47]. Previous studies have associated tumor heterogeneity with chemotherapeutic resistance and disease recurrence [71]. In the present study, we found substantially lower MATH score in LTS, suggesting less heterogeneous tumor tissue relative to STS and partially accounted for long-term survival.

Pathway analysis based on DEGs revealed that the olfactory transduction pathway was most significantly enriched. As a common clinical symptom in GBM patients, olfactory dysfunction has been proven to be associated with worse survival in a prospective case-control study regardless of

522 tumor location [72]. Furthermore, olfaction directly modulated glioma genesis in an autochthonous
523 mouse model [73]. The present study further highlighted the significance of olfactory transduction
524 genes in the course of GBM and suggested their potential of becoming novel biomarkers.
525 A striking finding of the present study is the identification of LTS tumors displaying remarkably
526 hypermethylated genome compared to STS counterparts. Among LGG, the glioma CpG island
527 methylator phenotype was demonstrated to be highly prevalent and linked with IDH mutation [74].
528 Although the patients we adopted were IDH-wildtype, the hypermethylation phenotype also
529 correlated with long-term survival. Furthermore, another resent study discovered that high global
530 DNA methylation correlated with improved survival in IDH-wildtype GBM [75]. The above
531 findings underlined similarity between certain GBM tumors and IDH-mutant glioma in terms of
532 global DNA methylation pattern. Further studies are required to elucidate the potential underlying
533 mechanism.
534 The TME of LTS tumors exhibited remarkably high infiltration of B cells, class-switched memory
535 B cells, M1 macrophages, $CD4^+$ Th1 cells and central memory $CD4^+$ T cells. A recent study on
536 breast cancer identified higher B cell infiltration to be associated with improved disease-free
537 survival. Moreover, class-switched memory B cells were found to be the most significant favorable
538 prognostic factor relative to other B cell subtypes [76]. Similarly, higher infiltration of class-
539 switched memory B cells in colorectal cancer was associated with better OS [77]. Considering
540 macrophages, M1 exerted anti-tumorigenic effects while M2 promoted immune evasion [78].
541 Similar to our results, a recent study of single-cell immune landscape observed M1 macrophage
542 accumulation in LTS GBM [49]. In addition, $CD4^+$ Th1 cells were proved to exert antitumor effects
543 and demonstrated higher infiltration in LTS relative to STS, while the opposite trend was observed

for $CD4^+$ Th2 cells which were known to favor tumor growth by inhibiting host immunity [79]. Central memory $CD4^+$ T cells not only protected host tissue from reinfection and cancer [80], but also correlated with favorable prognosis in oral squamous cell carcinoma [81]. Taken together, immune cell infiltration in LTS TME demonstrated higher antitumor activity compared to that of STS.

ICIs have demonstrated satisfying outcome in various advanced cancers, such as squamous cell lung cancer [82]. Similarly, combining programmed cell death-1 (PD-1) inhibitors with radiotherapy (RT) showed improved OS in multiple murine glioma models [83]. However, results from two phase III randomized studies (NCT02617589, NCT02667587) found Nivolumab, a PD-1 inhibitor, failed to bring additional benefit to newly diagnosed GBM patients treated with standard-of-care RT + TMZ regardless of *MGMT* promoter methylation status [84]. Therefore, it remains crucial to identify potential GBM responders to ICIs. Since TMB has been proposed as a potential predictor [82], our results of higher TMB in LTS suggested that these patients may get further benefit from ICI treatment.

Moreover, we identified a subset of STS, histologically diagnosed as GBM but matching diffuse pediatric-type high grade glioma based on methylation class, demonstrated poorer prognosis relative to STS m-GBM and lacked classical GBM molecular features. Previous studies mainly focused on this distinct subtype in pediatric patients, and the occurrence and clinical outcome in the adult population remains poorly understood [85].

Despite being the largest LTS cohort to date, one limitation of the present study is that the LTS sample size remains insufficient to thoroughly depict the molecular landscape of this GBM subclass. Future studies spanning multiple centers shall assist in gaining deeper understanding of LTS GBM.

In conclusion, the present study focused on a rare subset of IDH-wildtype GBM and incorporated the largest LTS cohort to date. WES, RNA-seq and DNA methylation array revealed distinct molecular profiles of LTS GBM including hypermethylated genome, copy number increase, less tumor heterogeneity, DEGs enriched in olfactory transduction, and higher antitumor immune activity. The above findings significantly advanced our understanding concerning the molecular profile of LTS GBM, and provided critical insights for improving molecular classification and developing novel therapeutic targets.

Funding

This work was supported by the National Natural Science Foundation of China (82103376) and Beijing Xisike Clinical Oncology Research Foundation (Y-zai2021/qn-0204 and Y-zai2021/zd-0207).

Author contributions

HX, XZ, LC, YM and ZQ conceived and designed the study. HX, XC and YS wrote the manuscript and prepared figures. XH, YW, QT, QZ, HC and XS provided patient data/material. YS and XZ did the bioinformatics analysis. YS, XZ, and KS performed experiments. YY, DZ, LC, YM and ZQ supervised the study. All authors contributed to and approved the final manuscript.

Declaration of competing interest

The authors declare that they have no known competing financial interests or personal relationships that could have appeared to influence the work reported in this paper.

Acknowledgments

We thank for the technical support from the Fudan University Shanghai Cancer Center.

Availability of data and materials

The raw data for WES, RNA sequencing, and BS-seq are accessible through the National Genomics Data Center (NGDC, https://ngdc.cncb.ac.cn/) of China. This information is cataloged under the Project ID PRJCA018782, subjected to controlled access. To obtain this data, please reach out either directly to the author or to the Data Access Committee (DAC) associated with the project.

References

[1] R. Stupp, W.P. Mason, M.J. van den Bent, M. Weller, B. Fisher, M.J. Taphoorn, K. Belanger, A.A. Brandes, C. Marosi, U. Bogdahn, J. Curschmann, R.C. Janzer, S.K. Ludwin, T. Gorlia, A. Allgeier, D. Lacombe, J.G. Cairncross, E. Eisenhauer, R.O. Mirimanoff, R. European Organisation for, T. Treatment of Cancer Brain, G. Radiotherapy, G. National Cancer Institute of Canada Clinical Trials, Radiotherapy plus concomitant and adjuvant temozolomide for glioblastoma, N Engl J Med, 352 (2005) 987-996.

[2] O.L. Chinot, W. Wick, W. Mason, R. Henriksson, F. Saran, R. Nishikawa, A.F. Carpentier, K. Hoang-Xuan, P. Kavan, D. Cernea, A.A. Brandes, M. Hilton, L. Abrey, T. Cloughesy, Bevacizumab plus radiotherapy-temozolomide for newly diagnosed glioblastoma, N Engl J Med, 370 (2014) 709-722.

[3] M.R. Gilbert, J.J. Dignam, T.S. Armstrong, J.S. Wefel, D.T. Blumenthal, M.A. Vogelbaum, H. Colman, A. Chakravarti, S. Pugh, M. Won, R. Jeraj, P.D. Brown, K.A. Jaeckle, D. Schiff, V.W. Stieber, D.G. Brachman, M. Werner-Wasik, I.W. Tremont-Lukats, E.P. Sulman, K.D. Aldape, W.J. Curran, Jr., M.P. Mehta, A randomized trial of bevacizumab for newly diagnosed glioblastoma, N Engl J Med, 370 (2014) 699-708.

[4] M.R. Gilbert, M. Wang, K.D. Aldape, R. Stupp, M.E. Hegi, K.A. Jaeckle, T.S. Armstrong, J.S. Wefel, M. Won, D.T. Blumenthal, A. Mahajan, C.J. Schultz, S. Erridge, B. Baumert, K.I. Hopkins, T. Tzuk-Shina, P.D. Brown, A. Chakravarti, W.J. Curran, Jr., M.P. Mehta, Dose-dense temozolomide for newly diagnosed glioblastoma: a randomized phase III clinical trial, J Clin Oncol, 31 (2013) 4085-4091.

[5] R. Stupp, S. Taillibert, A. Kanner, W. Read, D. Steinberg, B. Lhermitte, S. Toms, A. Idbaih, M.S. Ahluwalia, K. Fink, F. Di Meco, F. Lieberman, J.J. Zhu, G. Stragliotto, D. Tran, S. Brem, A. Hottinger, E.D. Kirson, G. Lavy-Shahaf, U. Weinberg, C.Y. Kim, S.H. Paek, G. Nicholas, J. Bruna, H. Hirte, M. Weller, Y. Palti, M.E. Hegi, Z. Ram, Effect of Tumor-Treating Fields Plus Maintenance Temozolomide vs Maintenance Temozolomide Alone on Survival in Patients With Glioblastoma: A Randomized Clinical Trial, JAMA, 318 (2017) 2306-2316.

[6] J.N. Cantrell, M.R. Waddle, M. Rotman, J.L. Peterson, H. Ruiz-Garcia, M.G. Heckman, A. Quinones-Hinojosa, S.S. Rosenfeld, P.D. Brown, D.M. Trifiletti, Progress Toward Long-Term Survivors of Glioblastoma, Mayo Clin Proc, 94 (2019) 1278-1286.

[7] T.J. Brown, M.C. Brennan, M. Li, E.W. Church, N.J. Brandmeir, K.L. Rakszawski, A.S. Patel, E.B. Rizk, D. Suki, R. Sawaya, M. Glantz, Association of the Extent of Resection With Survival in Glioblastoma: A Systematic Review and Meta-analysis, JAMA Oncol, 2 (2016) 1460-1469.

[8] A.C. Tan, D.M. Ashley, G.Y. Lopez, M. Malinzak, H.S. Friedman, M. Khasraw, Management of glioblastoma: State of the art and future directions, CA Cancer J Clin, 70 (2020) 299-312.

[9] M.G. Hart, R. Garside, G. Rogers, K. Stein, R. Grant, Temozolomide for high grade glioma, Cochrane Database Syst Rev, 2013 (2013) CD007415.

[10] Y. Ahmadipour, R. Jabbarli, O. Gembruch, D. Pierscianek, M. Darkwah Oppong, P. Dammann, K. Wrede, N. Ozkan, O. Muller, U. Sure, N. El Hindy, Impact of Multifocality and Molecular Markers on Survival of Glioblastoma, World Neurosurg, 122 (2019) e461-e466.

[11] H. Gittleman, Q.T. Ostrom, L.C. Stetson, K. Waite, T.R. Hodges, C.H. Wright, J. Wright, J.B. Rubin, M.E. Berens, J. Lathia, J.R. Connor, C. Kruchko, A.E. Sloan, J.S. Barnholtz-Sloan, Sex is an important prognostic factor for glioblastoma but not for nonglioblastoma, Neurooncol Pract, 6 (2019) 451-462.

[12] K. Ichimura, D.M. Pearson, S. Kocialkowski, L.M. Backlund, R. Chan, D.T. Jones, V.P. Collins, IDH1 mutations are present in the majority of common adult gliomas but rare in primary glioblastomas, Neuro Oncol, 11 (2009) 341-347.

[13] Y. Lu, J. Kwintkiewicz, Y. Liu, K. Tech, L.N. Frady, Y.T. Su, W. Bautista, S.I. Moon, J. MacDonald, M.G. Ewend, M.R. Gilbert, C. Yang, J. Wu, Chemosensitivity of IDH1-Mutated

Gliomas Due to an Impairment in PARP1-Mediated DNA Repair, Cancer Res, 77 (2017) 1709-1718.

[14] S. Lalezari, A.P. Chou, A. Tran, O.E. Solis, N. Khanlou, W. Chen, S. Li, J.A. Carrillo, R. Chowdhury, J. Selfridge, D.E. Sanchez, R.W. Wilson, M. Zurayk, J. Lalezari, J.J. Lou, L. Ormiston, K. Ancheta, R. Hanna, P. Miller, D. Piccioni, B.M. Ellingson, C. Buchanan, P.S. Mischel, P.L. Nghiemphu, R. Green, H.J. Wang, W.B. Pope, L.M. Liau, R.M. Elashoff, T.F. Cloughesy, W.H. Yong, A. Lai, Combined analysis of O6-methylguanine-DNA methyltransferase protein expression and promoter methylation provides optimized prognostication of glioblastoma outcome, Neuro Oncol, 15 (2013) 370-381.

[15] D.J. Brat, K. Aldape, H. Colman, E.C. Holland, D.N. Louis, R.B. Jenkins, B.K. Kleinschmidt-DeMasters, A. Perry, G. Reifenberger, R. Stupp, A. von Deimling, M. Weller, cIMPACT-NOW update 3: recommended diagnostic criteria for "Diffuse astrocytic glioma, IDH-wildtype, with molecular features of glioblastoma, WHO grade IV", Acta Neuropathol, 136 (2018) 805-810.

[16] D. Stichel, A. Ebrahimi, D. Reuss, D. Schrimpf, T. Ono, M. Shirahata, G. Reifenberger, M. Weller, D. Hanggi, W. Wick, C. Herold-Mende, M. Westphal, S. Brandner, S.M. Pfister, D. Capper, F. Sahm, A. von Deimling, Distribution of EGFR amplification, combined chromosome 7 gain and chromosome 10 loss, and TERT promoter mutation in brain tumors and their potential for the reclassification of IDHwt astrocytoma to glioblastoma, Acta Neuropathol, 136 (2018) 793-803.

[17] F. Zeng, K. Wang, R. Huang, Y. Liu, Y. Zhang, H. Hu, RELB: A novel prognostic marker for glioblastoma as identified by population-based analysis, Oncol Lett, 18 (2019) 386-394.

[18] N. Cancer Genome Atlas Research, D.J. Brat, R.G. Verhaak, K.D. Aldape, W.K. Yung, S.R. Salama, L.A. Cooper, E. Rheinbay, C.R. Miller, M. Vitucci, O. Morozova, A.G. Robertson, H. Noushmehr, P.W. Laird, A.D. Cherniack, R. Akbani, J.T. Huse, G. Ciriello, L.M. Poisson, J.S. Barnholtz-Sloan, M.S. Berger, C. Brennan, R.R. Colen, H. Colman, A.E. Flanders, C. Giannini, M. Grifford, A. Iavarone, R. Jain, I. Joseph, J. Kim, K. Kasaian, T. Mikkelsen, B.A. Murray, B.P. O'Neill, L. Pachter, D.W. Parsons, C. Sougnez, E.P. Sulman, S.R. Vandenberg, E.G. Van Meir, A. von Deimling, H. Zhang, D. Crain, K. Lau, D. Mallery, S. Morris, J. Paulauskis, R. Penny, T. Shelton, M. Sherman, P. Yena, A. Black, J. Bowen, K. Dicostanzo, J. Gastier-Foster, K.M. Leraas, T.M. Lichtenberg, C.R. Pierson, N.C. Ramirez, C. Taylor, S. Weaver, L. Wise, E. Zmuda, T. Davidsen, J.A. Demchok, G. Eley, M.L. Ferguson, C.M. Hutter, K.R. Mills Shaw, B.A. Ozenberger, M. Sheth, H.J. Sofia, R. Tarnuzzer, Z. Wang, L. Yang, J.C. Zenklusen, B. Ayala, J. Baboud, S. Chudamani, M.A. Jensen, J. Liu, T. Pihl, R. Raman, Y. Wan, Y. Wu, A. Ally, J.T. Auman, M. Balasundaram, S. Balu, S.B. Baylin, R. Beroukhim, M.S. Bootwalla, R. Bowlby, C.A. Bristow, D.

Brooks, Y. Butterfield, R. Carlsen, S. Carter, L. Chin, A. Chu, E. Chuah, K. Cibulskis, A. Clarke, S.G. Coetzee, N. Dhalla, T. Fennell, S. Fisher, S. Gabriel, G. Getz, R. Gibbs, R. Guin, A. Hadjipanayis, D.N. Hayes, T. Hinoue, K. Hoadley, R.A. Holt, A.P. Hoyle, S.R. Jefferys, S. Jones, C.D. Jones, R. Kucherlapati, P.H. Lai, E. Lander, S. Lee, L. Lichtenstein, Y. Ma, D.T. Maglinte, H.S. Mahadeshwar, M.A. Marra, M. Mayo, S. Meng, M.L. Meyerson, P.A. Mieczkowski, R.A. Moore, L.E. Mose, A.J. Mungall, A. Pantazi, M. Parfenov, P.J. Park, J.S. Parker, C.M. Perou, A. Protopopov, X. Ren, J. Roach, T.S. Sabedot, J. Schein, S.E. Schumacher, J.G. Seidman, S. Seth, H. Shen, J.V. Simons, P. Sipahimalani, M.G. Soloway, X. Song, H. Sun, B. Tabak, A. Tam, D. Tan, J. Tang, N. Thiessen, T. Triche, Jr., D.J. Van Den Berg, U. Veluvolu, S. Waring, D.J. Weisenberger, M.D. Wilkerson, T. Wong, J. Wu, L. Xi, A.W. Xu, L. Yang, T.I. Zack, J. Zhang, B.A. Aksoy, H. Arachchi, C. Benz, B. Bernard, D. Carlin, J. Cho, D. DiCara, S. Frazer, G.N. Fuller, J. Gao, N. Gehlenborg, D. Haussler, D.I. Heiman, L. Iype, A. Jacobsen, Z. Ju, S. Katzman, H. Kim, T. Knijnenburg, R.B. Kreisberg, M.S. Lawrence, W. Lee, K. Leinonen, P. Lin, S. Ling, W. Liu, Y. Liu, Y. Liu, Y. Lu, G. Mills, S. Ng, M.S. Noble, E. Paull, A. Rao, S. Reynolds, G. Saksena, Z. Sanborn, C. Sander, N. Schultz, Y. Senbabaoglu, R. Shen, I. Shmulevich, R. Sinha, J. Stuart, S.O. Sumer, Y. Sun, N. Tasman, B.S. Taylor, D. Voet, N. Weinhold, J.N. Weinstein, D. Yang, K. Yoshihara, S. Zheng, W. Zhang, L. Zou, T. Abel, S. Sadeghi, M.L. Cohen, J. Eschbacher, E.M. Hattab, A. Raghunathan, M.J. Schniederjan, D. Aziz, G. Barnett, W. Barrett, D.D. Bigner, L. Boice, C. Brewer, C. Calatozzolo, B. Campos, C.G. Carlotti, Jr., T.A. Chan, L. Cuppini, E. Curley, S. Cuzzubbo, K. Devine, F. DiMeco, R. Duell, J.B. Elder, A. Fehrenbach, G. Finocchiaro, W. Friedman, J. Fulop, J. Gardner, B. Hermes, C. Herold-Mende, C. Jungk, A. Kendler, N.L. Lehman, E. Lipp, O. Liu, R. Mandt, M. McGraw, R. McLendon, C. McPherson, L. Neder, P. Nguyen, A. Noss, R. Nunziata, Q.T. Ostrom, C. Palmer, A. Perin, B. Pollo, A. Potapov, O. Potapova, W.K. Rathmell, D. Rotin, L. Scarpace, C. Schilero, K. Senecal, K. Shimmel, V. Shurkhay, S. Sifri, R. Singh, A.E. Sloan, K. Smolenski, S.M. Staugaitis, R. Steele, L. Thorne, D.P. Tirapelli, A. Unterberg, M. Vallurupalli, Y. Wang, R. Warnick, F. Williams, Y. Wolinsky, S. Bell, M. Rosenberg, C. Stewart, F. Huang, J.L. Grimsby, A.J. Radenbaugh, J. Zhang, Comprehensive, Integrative Genomic Analysis of Diffuse Lower-Grade Gliomas, N Engl J Med, 372 (2015) 2481-2498.

[19] B. Wiestler, D. Capper, T. Holland-Letz, A. Korshunov, A. von Deimling, S.M. Pfister, M. Platten, M. Weller, W. Wick, ATRX loss refines the classification of anaplastic gliomas and identifies a subgroup of IDH mutant astrocytic tumors with better prognosis, Acta Neuropathol, 126 (2013) 443-451.

[20] S.R. Michaelsen, T. Urup, L.R. Olsen, H. Broholm, U. Lassen, H.S. Poulsen, Molecular profiling of short-term and long-term surviving patients identifies CD34 mRNA level as prognostic for glioblastoma survival, J Neurooncol, 137 (2018) 533-542.

[21] D.M. Burgenske, J. Yang, P.A. Decker, T.M. Kollmeyer, M.L. Kosel, A.C. Mladek, A.A. Caron, R.A. Vaubel, S.K. Gupta, G.J. Kitange, H. Sicotte, R.S. Youland, D. Remonde, J.S. Voss, E.G.B. Fritcher, K.L. Kolsky, C.M. Ida, F.B. Meyer, D.H. Lachance, I.J. Parney, B.R. Kipp, C. Giannini, E.P. Sulman, R.B. Jenkins, J.E. Eckel-Passow, J.N. Sarkaria, Molecular profiling of long-term IDH-wildtype glioblastoma survivors, Neuro Oncol, 21 (2019) 1458-1469.

[22] D. Cantero, A. Rodriguez de Lope, R. Moreno de la Presa, J.M. Sepulveda, J.M. Borras, J.S. Castresana, N. D'Haene, J.F. Garcia, I. Salmon, M. Mollejo, J.A. Rey, A. Hernandez-Lain, B. Melendez, Molecular Study of Long-Term Survivors of Glioblastoma by Gene-Targeted Next-Generation Sequencing, J Neuropathol Exp Neurol, 77 (2018) 710-716.

[23] D.N. Louis, A. Perry, P. Wesseling, D.J. Brat, I.A. Cree, D. Figarella-Branger, C. Hawkins, H.K. Ng, S.M. Pfister, G. Reifenberger, R. Soffietti, A. von Deimling, D.W. Ellison, The 2021 WHO Classification of Tumors of the Central Nervous System: a summary, Neuro Oncol, 23 (2021) 1231-1251.

[24] A. Aibaidula, J.F. Lu, J.S. Wu, H.J. Zou, H. Chen, Y.Q. Wang, Z.Y. Qin, Y. Yao, Y. Gong, X.M. Che, P. Zhong, S.Q. Li, W.M. Bao, Y. Mao, L.F. Zhou, Establishment and maintenance of a standardized glioma tissue bank: Huashan experience, Cell Tissue Bank, 16 (2015) 271-281.

[25] H. Li, R. Durbin, Fast and accurate short read alignment with Burrows-Wheeler transform, Bioinformatics, 25 (2009) 1754-1760.

[26] K.I. Kendig, S. Baheti, M.A. Bockol, T.M. Drucker, S.N. Hart, J.R. Heldenbrand, M. Hernaez, M.E. Hudson, M.T. Kalmbach, E.W. Klee, N.R. Mattson, C.A. Ross, M. Taschuk, E.D. Wieben, M. Wiepert, D.E. Wildman, L.S. Mainzer, Sentieon DNASeq Variant Calling Workflow Demonstrates Strong Computational Performance and Accuracy, Front Genet, 10 (2019) 736.

[27] W. McLaren, L. Gil, S.E. Hunt, H.S. Riat, G.R. Ritchie, A. Thormann, P. Flicek, F. Cunningham, The Ensembl Variant Effect Predictor, Genome Biol, 17 (2016) 122.

[28] E.A. Mroz, A.D. Tward, R.J. Hammon, Y. Ren, J.W. Rocco, Intra-tumor genetic heterogeneity and mortality in head and neck cancer: analysis of data from the Cancer Genome Atlas, PLoS Med, 12 (2015) e1001786.

[29] A. Mayakonda, D.C. Lin, Y. Assenov, C. Plass, H.P. Koeffler, Maftools: efficient and comprehensive analysis of somatic variants in cancer, Genome Res, 28 (2018) 1747-1756.

[30] J.F. Sathirapongsasuti, H. Lee, B.A. Horst, G. Brunner, A.J. Cochran, S. Binder, J. Quackenbush, S.F. Nelson, Exome sequencing-based copy-number variation and loss of heterozygosity detection: ExomeCNV, Bioinformatics, 27 (2011) 2648-2654.

[31] B. Niu, K. Ye, Q. Zhang, C. Lu, M. Xie, M.D. McLellan, M.C. Wendl, L. Ding, MSIsensor: microsatellite instability detection using paired tumor-normal sequence data, Bioinformatics, 30 (2014) 1015-1016.

[32] S. Kovaka, A.V. Zimin, G.M. Pertea, R. Razaghi, S.L. Salzberg, M. Pertea, Transcriptome assembly from long-read RNA-seq alignments with StringTie2, Genome Biol, 20 (2019) 278.

[33] A. Dobin, C.A. Davis, F. Schlesinger, J. Drenkow, C. Zaleski, S. Jha, P. Batut, M. Chaisson, T.R. Gingeras, STAR: ultrafast universal RNA-seq aligner, Bioinformatics, 29 (2013) 15-21.

[34] M.I. Love, W. Huber, S. Anders, Moderated estimation of fold change and dispersion for RNA-seq data with DESeq2, Genome Biol, 15 (2014) 550.

[35] M. Kanehisa, S. Goto, KEGG: kyoto encyclopedia of genes and genomes, Nucleic Acids Res, 28 (2000) 27-30.

[36] C. Gene Ontology, S.A. Aleksander, J. Balhoff, S. Carbon, J.M. Cherry, H.J. Drabkin, D. Ebert, M. Feuermann, P. Gaudet, N.L. Harris, D.P. Hill, R. Lee, H. Mi, S. Moxon, C.J. Mungall, A. Muruganugan, T. Mushayahama, P.W. Sternberg, P.D. Thomas, K. Van Auken, J. Ramsey, D.A. Siegele, R.L. Chisholm, P. Fey, M.C. Aspromonte, M.V. Nugnes, F. Quaglia, S. Tosatto, M. Giglio, S. Nadendla, G. Antonazzo, H. Attrill, G. Dos Santos, S. Marygold, V. Strelets, C.J. Tabone, J. Thurmond, P. Zhou, S.H. Ahmed, P. Asanitthong, D. Luna Buitrago, M.N. Erdol, M.C. Gage, M. Ali Kadhum, K.Y.C. Li, M. Long, A. Michalak, A. Pesala, A. Pritazahra, S.C.C. Saverimuttu, R. Su, K.E. Thurlow, R.C. Lovering, C. Logie, S. Oliferenko, J. Blake, K. Christie, L. Corbani, M.E. Dolan, H.J. Drabkin, D.P. Hill, L. Ni, D. Sitnikov, C. Smith, A. Cuzick, J. Seager, L. Cooper, J. Elser, P. Jaiswal, P. Gupta, P. Jaiswal, S. Naithani, M. Lera-Ramirez, K. Rutherford, V. Wood, J.L. De Pons, M.R. Dwinell, G.T. Hayman, M.L. Kaldunski, A.E. Kwitek, S.J.F. Laulederkind, M.A. Tutaj, M. Vedi, S.J. Wang, P. D'Eustachio, L. Aimo, K. Axelsen, A. Bridge, N. Hyka-Nouspikel, A. Morgat, S.A. Aleksander, J.M. Cherry, S.R. Engel, K. Karra, S.R. Miyasato, R.S. Nash, M.S. Skrzypek, S. Weng, E.D. Wong, E. Bakker, T.Z. Berardini, L. Reiser, A. Auchincloss, K. Axelsen, G. Argoud-Puy, M.C. Blatter, E. Boutet, L. Breuza, A. Bridge, C. Casals-Casas, E. Coudert, A. Estreicher, M. Livia Famiglietti, M. Feuermann, A. Gos, N. Gruaz-Gumowski, C. Hulo, N. Hyka-Nouspikel, F. Jungo, P. Le Mercier, D. Lieberherr, P. Masson, A. Morgat, I. Pedruzzi, L. Pourcel, S. Poux, C. Rivoire, S. Sundaram, A. Bateman, E. Bowler-Barnett, A.J.H. Bye, P. Denny, A. Ignatchenko, R. Ishtiaq, A. Lock, Y. Lussi, M. Magrane, M.J. Martin, S. Orchard, P. Raposo, E.

Speretta, N. Tyagi, K. Warner, R. Zaru, A.D. Diehl, R. Lee, J. Chan, S. Diamantakis, D. Raciti, M. Zarowiecki, M. Fisher, C. James-Zorn, V. Ponferrada, A. Zorn, S. Ramachandran, L. Ruzicka, M. Westerfield, The Gene Ontology knowledgebase in 2023, Genetics, 224 (2023).

[37] D. Aran, Z. Hu, A.J. Butte, xCell: digitally portraying the tissue cellular heterogeneity landscape, Genome Biol, 18 (2017) 220.

[38] Z. Gu, R. Eils, M. Schlesner, Complex heatmaps reveal patterns and correlations in multidimensional genomic data, Bioinformatics, 32 (2016) 2847-2849.

[39] H. Wickham, ggplot2: elegant graphics for data analysis New York, NY: Springer, (2009).

[40] C.H. Mermel, S.E. Schumacher, B. Hill, M.L. Meyerson, R. Beroukhim, G. Getz, GISTIC2.0 facilitates sensitive and confident localization of the targets of focal somatic copy-number alteration in human cancers, Genome Biol, 12 (2011) R41.

[41] B.J. Haas, A. Dobin, B. Li, N. Stransky, N. Pochet, A. Regev, Accuracy assessment of fusion transcript detection via read-mapping and de novo fusion transcript assembly-based methods, Genome Biol, 20 (2019) 213.

[42] M.D. Wilkerson, D.N. Hayes, ConsensusClusterPlus: a class discovery tool with confidence assessments and item tracking, Bioinformatics, 26 (2010) 1572-1573.

[43] R. Kolde, Pheatmap: Pretty Heatmaps; R Package Version 1.0. 12; CRAN, R-Project, 2019.

[44] T.J. Morris, L.M. Butcher, A. Feber, A.E. Teschendorff, A.R. Chakravarthy, T.K. Wojdacz, S. Beck, ChAMP: 450k Chip Analysis Methylation Pipeline, Bioinformatics, 30 (2014) 428-430.

[45] W. Timp, H.C. Bravo, O.G. McDonald, M. Goggins, C. Umbricht, M. Zeiger, A.P. Feinberg, R.A. Irizarry, Large hypomethylated blocks as a universal defining epigenetic alteration in human solid tumors, Genome Med, 6 (2014) 61.

[46] F. Pedregosa, G. Varoquaux, A. Gramfort, V. Michel, B. Thirion, O. Grisel, M. Blondel, P. Prettenhofer, R. Weiss, V. Dubourg, Scikit-learn: Machine learning in Python, the Journal of machine Learning research, 12 (2011) 2825-2830.

[47] D. Capper, D.T.W. Jones, M. Sill, V. Hovestadt, D. Schrimpf, D. Sturm, C. Koelsche, F. Sahm, L. Chavez, D.E. Reuss, A. Kratz, A.K. Wefers, K. Huang, K.W. Pajtler, L. Schweizer, D. Stichel, A. Olar, N.W. Engel, K. Lindenberg, P.N. Harter, A.K. Braczynski, K.H. Plate, H. Dohmen, B.K. Garvalov, R. Coras, A. Holsken, E. Hewer, M. Bewerunge-Hudler, M. Schick, R. Fischer, R. Beschorner, J. Schittenhelm, O. Staszewski, K. Wani, P. Varlet, M. Pages, P. Temming, D. Lohmann, F. Selt, H. Witt, T. Milde, O. Witt, E. Aronica, F. Giangaspero, E. Rushing, W. Scheurlen, C. Geisenberger, F.J. Rodriguez, A. Becker, M. Preusser, C. Haberler, R. Bjerkvig, J. Cryan, M. Farrell, M. Deckert, J. Hench, S. Frank, J. Serrano, K. Kannan, A. Tsirigos, W. Bruck, S. Hofer, S.

Brehmer, M. Seiz-Rosenhagen, D. Hanggi, V. Hans, S. Rozsnoki, J.R. Hansford, P. Kohlhof, B.W. Kristensen, M. Lechner, B. Lopes, C. Mawrin, R. Ketter, A. Kulozik, Z. Khatib, F. Heppner, A. Koch, A. Jouvet, C. Keohane, H. Muhleisen, W. Mueller, U. Pohl, M. Prinz, A. Benner, M. Zapatka, N.G. Gottardo, P.H. Driever, C.M. Kramm, H.L. Muller, S. Rutkowski, K. von Hoff, M.C. Fruhwald, A. Gnekow, G. Fleischhack, S. Tippelt, G. Calaminus, C.M. Monoranu, A. Perry, C. Jones, T.S. Jacques, B. Radlwimmer, M. Gessi, T. Pietsch, J. Schramm, G. Schackert, M. Westphal, G. Reifenberger, P. Wesseling, M. Weller, V.P. Collins, I. Blumcke, M. Bendszus, J. Debus, A. Huang, N. Jabado, P.A. Northcott, W. Paulus, A. Gajjar, G.W. Robinson, M.D. Taylor, Z. Jaunmuktane, M. Ryzhova, M. Platten, A. Unterberg, W. Wick, M.A. Karajannis, M. Mittelbronn, T. Acker, C. Hartmann, K. Aldape, U. Schuller, R. Buslei, P. Lichter, M. Kool, C. Herold-Mende, D.W. Ellison, M. Hasselblatt, M. Snuderl, S. Brandner, A. Korshunov, A. von Deimling, S.M. Pfister, DNA methylation-based classification of central nervous system tumours, Nature, 555 (2018) 469-474.

[48] T. Komori, Beyond the WHO 2021 classification of the tumors of the central nervous system: transitioning from the 5th edition to the next, Brain Tumor Pathol, (2023).

[49] E. Karimi, M.W. Yu, S.M. Maritan, L.J.M. Perus, M. Rezanejad, M. Sorin, M. Dankner, P. Fallah, S. Dore, D. Zuo, B. Fiset, D.J. Kloosterman, L. Ramsay, Y. Wei, S. Lam, R. Alsajjan, I.R. Watson, G. Roldan Urgoiti, M. Park, D. Brandsma, D.L. Senger, J.A. Chan, L. Akkari, K. Petrecca, M.C. Guiot, P.M. Siegel, D.F. Quail, L.A. Walsh, Single-cell spatial immune landscapes of primary and metastatic brain tumours, Nature, 614 (2023) 555-563.

[50] P. Ofek, E. Yeini, G. Arad, A. Danilevsky, S. Pozzi, C.B. Luna, S.I. Dangoor, R. Grossman, Z. Ram, N. Shomron, H. Brem, T.M. Hyde, T. Geiger, R. Satchi-Fainaro, Deoxyhypusine hydroxylase: A novel therapeutic target differentially expressed in short-term vs long-term survivors of glioblastoma, Int J Cancer, 153 (2023) 654-668.

[51] G. Chehade, T.M. Lawson, J. Lelotte, L. Daoud, D. Di Perri, N. Whenham, T. Duprez, N. Tajeddine, F. Tissir, C. Raftopoulos, Long-term survival in patients with IDH-wildtype glioblastoma: clinical and molecular characteristics, Acta Neurochir (Wien), 165 (2023) 1075-1085.

[52] B. Schneider, N. Lamp, A. Zimpfer, C. Henker, A. Erbersdobler, Comparing tumor microRNA profiles of patients with long- and short-term-surviving glioblastoma, Mol Med Rep, 27 (2023).

[53] V.N. Sommerlath, D. Buergy, N. Etminan, S. Brehmer, D. Reuss, G.R. Sarria, M.C. Guiot, D. Hanggi, F. Wenz, K. Petrecca, F.A. Giordano, Molecular features of glioblastomas in long-term survivors compared to short-term survivors-a matched-pair analysis, Radiat Oncol, 17 (2022) 15.

[54] H. Jiang, K. Yu, Y. Cui, X. Ren, M. Li, G. Zhang, C. Yang, X. Zhao, Q. Zhu, S. Lin, Differential Predictors and Clinical Implications Associated With Long-Term Survivors in IDH Wildtype and Mutant Glioblastoma, Front Oncol, 11 (2021) 632663.

[55] L. Yu, G. Zhang, S. Qi, Aggressive Treatment in Glioblastoma: What Determines the Survival of Patients?, J Neurol Surg A Cent Eur Neurosurg, 82 (2021) 112-117.

[56] V.S. Madhugiri, A.V. Moiyadi, P. Shetty, T. Gupta, S. Epari, R. Jalali, V. Subeikshanan, A. Dutt, G.M. Sasidharan, V.R. Roopesh Kumar, C.V. Shankar Ganesh, A.S. Ramesh, A. Sathia Prabhu, Analysis of Factors Associated with Long-Term Survival in Patients with Glioblastoma, World Neurosurg, 149 (2021) e758-e765.

[57] E. Marton, E. Giordan, F. Siddi, C. Curzi, G. Canova, B. Scarpa, A. Guerriero, S. Rossi, D.A. D, P. Longatti, A. Feletti, Over ten years overall survival in glioblastoma: A different disease?, J Neurol Sci, 408 (2020) 116518.

[58] T.E. Richardson, S. Patel, J. Serrano, A.A. Sathe, E.V. Daoud, D. Oliver, E.A. Maher, A. Madrigales, B.E. Mickey, T. Taxter, G. Jour, C.L. White, J.M. Raisanen, C. Xing, M. Snuderl, K.J. Hatanpaa, Genome-Wide Analysis of Glioblastoma Patients with Unexpectedly Long Survival, J Neuropathol Exp Neurol, 78 (2019) 501-507.

[59] D. Armocida, A. Pesce, F. Di Giammarco, A. Frati, A. Santoro, M. Salvati, Long Term Survival in Patients Suffering from Glio-blastoma Multiforme: A Single-Center Observational Cohort Study, Diagnostics (Basel), 9 (2019).

[60] T. Hwang, D. Mathios, K.L. McDonald, I. Daris, S.H. Park, P.C. Burger, S. Kim, Y.S. Dho, H. Carolyn, C. Bettegowda, J.H. Shin, M. Lim, C.K. Park, Integrative analysis of DNA methylation suggests down-regulation of oncogenic pathways and reduced somatic mutation rates in survival outliers of glioblastoma, Acta Neuropathol Commun, 7 (2019) 88.

[61] E. Aquilanti, J. Miller, S. Santagata, D.P. Cahill, P.K. Brastianos, Updates in prognostic markers for gliomas, Neuro Oncol, 20 (2018) vii17-vii26.

[62] J. Li, R. Liang, C. Song, Y. Xiang, Y. Liu, Prognostic significance of epidermal growth factor receptor expression in glioma patients, Onco Targets Ther, 11 (2018) 731-742.

[63] B.K. Kleinschmidt-DeMasters, D.L. Aisner, D.K. Birks, N.K. Foreman, Epithelioid GBMs show a high percentage of BRAF V600E mutation, Am J Surg Pathol, 37 (2013) 685-698.

[64] Y. Suzuki, J. Takahashi-Fujigasaki, Y. Akasaki, S. Matsushima, R. Mori, K. Karagiozov, T. Joki, S. Ikeuchi, M. Ikegami, Y. Manome, Y. Murayama, BRAF V600E-mutated diffuse glioma in an adult patient: a case report and review, Brain Tumor Pathol, 33 (2016) 40-49.

[65] M. Weller, M. van den Bent, M. Preusser, E. Le Rhun, J.C. Tonn, G. Minniti, M. Bendszus, C. Balana, O. Chinot, L. Dirven, P. French, M.E. Hegi, A.S. Jakola, M. Platten, P. Roth, R. Ruda, S. Short, M. Smits, M.J.B. Taphoorn, A. von Deimling, M. Westphal, R. Soffietti, G. Reifenberger, W. Wick, EANO guidelines on the diagnosis and treatment of diffuse gliomas of adulthood, Nat Rev Clin Oncol, 18 (2021) 170-186.

[66] F. Oswald, U. Kostezka, K. Astrahantseff, S. Bourteele, K. Dillinger, U. Zechner, L. Ludwig, M. Wilda, H. Hameister, W. Knochel, S. Liptay, R.M. Schmid, SHARP is a novel component of the Notch/RBP-Jkappa signalling pathway, EMBO J, 21 (2002) 5417-5426.

[67] Q. Liu, X.Y. Wang, Y.Y. Qin, X.L. Yan, H.M. Chen, Q.D. Huang, J.K. Chen, J.M. Zheng, SPOCD1 promotes the proliferation and metastasis of glioma cells by up-regulating PTX3, Am J Cancer Res, 8 (2018) 624-635.

[68] G. Iegiani, F. Di Cunto, G. Pallavicini, Inhibiting microcephaly genes as alternative to microtubule targeting agents to treat brain tumors, Cell Death Dis, 12 (2021) 956.

[69] Y.N. Urata, F. Takeshita, H. Tanaka, T. Ochiya, M. Takimoto, Targeted Knockdown of the Kinetochore Protein D40/Knl-1 Inhibits Human Cancer in a p53 Status-Independent Manner, Sci Rep, 5 (2015) 13676.

[70] H. Hu, Q. Mu, Z. Bao, Y. Chen, Y. Liu, J. Chen, K. Wang, Z. Wang, Y. Nam, B. Jiang, J.K. Sa, H.J. Cho, N.G. Her, C. Zhang, Z. Zhao, Y. Zhang, F. Zeng, F. Wu, X. Kang, Y. Liu, Z. Qian, Z. Wang, R. Huang, Q. Wang, W. Zhang, X. Qiu, W. Li, D.H. Nam, X. Fan, J. Wang, T. Jiang, Mutational Landscape of Secondary Glioblastoma Guides MET-Targeted Trial in Brain Tumor, Cell, 175 (2018) 1665-1678 e1618.

[71] C. Neftel, J. Laffy, M.G. Filbin, T. Hara, M.E. Shore, G.J. Rahme, A.R. Richman, D. Silverbush, M.L. Shaw, C.M. Hebert, J. Dewitt, S. Gritsch, E.M. Perez, L.N. Gonzalez Castro, X. Lan, N. Druck, C. Rodman, D. Dionne, A. Kaplan, M.S. Bertalan, J. Small, K. Pelton, S. Becker, D. Bonal, Q.D. Nguyen, R.L. Servis, J.M. Fung, R. Mylvaganam, L. Mayr, J. Gojo, C. Haberler, R. Geyeregger, T. Czech, I. Slavc, B.V. Nahed, W.T. Curry, B.S. Carter, H. Wakimoto, P.K. Brastianos, T.T. Batchelor, A. Stemmer-Rachamimov, M. Martinez-Lage, M.P. Frosch, I. Stamenkovic, N. Riggi, E. Rheinbay, M. Monje, O. Rozenblatt-Rosen, D.P. Cahill, A.P. Patel, T. Hunter, I.M. Verma, K.L. Ligon, D.N. Louis, A. Regev, B.E. Bernstein, I. Tirosh, M.L. Suva, An Integrative Model of Cellular States, Plasticity, and Genetics for Glioblastoma, Cell, 178 (2019) 835-849 e821.

[72] S. Kebir, E. Hattingen, M. Niessen, L. Rauschenbach, R. Fimmers, T. Hummel, N. Schafer, L. Lazaridis, C. Kleinschnitz, U. Herrlinger, B. Scheffler, M. Glas, Olfactory function as an independent prognostic factor in glioblastoma, Neurology, 94 (2020) e529-e537.

[73] P. Chen, W. Wang, R. Liu, J. Lyu, L. Zhang, B. Li, B. Qiu, A. Tian, W. Jiang, H. Ying, R. Jing, Q. Wang, K. Zhu, R. Bai, L. Zeng, S. Duan, C. Liu, Olfactory sensory experience regulates gliomagenesis via neuronal IGF1, Nature, 606 (2022) 550-556.

[74] S. Turcan, D. Rohle, A. Goenka, L.A. Walsh, F. Fang, E. Yilmaz, C. Campos, A.W. Fabius, C. Lu, P.S. Ward, C.B. Thompson, A. Kaufman, O. Guryanova, R. Levine, A. Heguy, A. Viale, L.G. Morris, J.T. Huse, I.K. Mellinghoff, T.A. Chan, IDH1 mutation is sufficient to establish the glioma hypermethylator phenotype, Nature, 483 (2012) 479-483.

[75] A. Eckhardt, R. Drexler, M. Schoof, N. Struve, D. Capper, C. Jelgersma, J. Onken, P.N. Harter, K.J. Weber, I. Dive, K. Rothkamm, K. Hoffer, L. Klumpp, K. Ganser, C. Petersen, F. Ricklefs, M. Kriegs, U. Schuller, Mean global DNA methylation serves as independent prognostic marker in IDH-wildtype glioblastoma, Neuro Oncol, 26 (2024) 503-513.

[76] Mariko Asaoka, Rongrong Wu, Takashi Ishikawa (2023) Increased infiltrating class-switched memory B cell in breast cancer tumors were associated with favorable prognostic outcome [abstract]. In: Proceedings of the American Association for Cancer Research Annual Meeting 2023; Part 1 (Regular and Invited Abstracts); 2023 Apr 14-19; Orlando, FL. Philadelphia (PA): AACR; Cancer Res 2023;83(7_Suppl):Abstract nr 1408.

[77] F.J. Hansen, Z. Wu, P. David, A. Mittelstadt, A. Jacobsen, M.J. Podolska, K. Ubieta, M. Brunner, D. Kouhestani, I. Swierzy, L. Rossdeutsch, B. Klosch, I. Kutschick, S. Merkel, A. Denz, K. Weber, C. Geppert, R. Grutzmann, A. Benard, G.F. Weber, Tumor Infiltration with CD20(+)CD73(+) B Cells Correlates with Better Outcome in Colorectal Cancer, Int J Mol Sci, 23 (2022).

[78] S. Mahajan, M.H.H. Schmidt, U. Schumann, The Glioma Immune Landscape: A Double-Edged Sword for Treatment Regimens, Cancers (Basel), 15 (2023).

[79] M. Mateu-Jimenez, V. Curull, L. Pijuan, A. Sanchez-Font, H. Rivera-Ramos, A. Rodriguez-Fuster, R. Aguilo, J. Gea, E. Barreiro, Systemic and Tumor Th1 and Th2 Inflammatory Profile and Macrophages in Lung Cancer: Influence of Underlying Chronic Respiratory Disease, J Thorac Oncol, 12 (2017) 235-248.

[80] M. Kunzli, D. Masopust, CD4(+) T cell memory, Nat Immunol, 24 (2023) 903-914.

[81] J. Wu, T. Zhang, H. Xiong, L. Zeng, Z. Wang, Y. Peng, W. Chen, X. Hu, T. Su, Tumor-Infiltrating CD4(+) Central Memory T Cells Correlated with Favorable Prognosis in Oral Squamous Cell Carcinoma, J Inflamm Res, 15 (2022) 141-152.

[82] J. Brahmer, K.L. Reckamp, P. Baas, L. Crino, W.E. Eberhardt, E. Poddubskaya, S. Antonia, A. Pluzanski, E.E. Vokes, E. Holgado, D. Waterhouse, N. Ready, J. Gainor, O. Aren Frontera, L. Havel,

M. Steins, M.C. Garassino, J.G. Aerts, M. Domine, L. Paz-Ares, M. Reck, C. Baudelet, C.T. Harbison, B. Lestini, D.R. Spigel, Nivolumab versus Docetaxel in Advanced Squamous-Cell Non-Small-Cell Lung Cancer, N Engl J Med, 373 (2015) 123-135.

[83] J. Zeng, A.P. See, J. Phallen, C.M. Jackson, Z. Belcaid, J. Ruzevick, N. Durham, C. Meyer, T.J. Harris, E. Albesiano, G. Pradilla, E. Ford, J. Wong, H.J. Hammers, D. Mathios, B. Tyler, H. Brem, P.T. Tran, D. Pardoll, C.G. Drake, M. Lim, Anti-PD-1 blockade and stereotactic radiation produce long-term survival in mice with intracranial gliomas, Int J Radiat Oncol Biol Phys, 86 (2013) 343-349.

[84] M. Lim, M. Weller, A. Idbaih, J. Steinbach, G. Finocchiaro, R.R. Raval, G. Ansstas, J. Baehring, J.W. Taylor, J. Honnorat, K. Petrecca, F. De Vos, A. Wick, A. Sumrall, S. Sahebjam, I.K. Mellinghoff, M. Kinoshita, M. Roberts, R. Slepetis, D. Warad, D. Leung, M. Lee, D.A. Reardon, A. Omuro, Phase III trial of chemoradiotherapy with temozolomide plus nivolumab or placebo for newly diagnosed glioblastoma with methylated MGMT promoter, Neuro Oncol, 24 (2022) 1935-1949.

[85] K. Bender, J. Kahn, E. Perez, F. Ehret, S. Roohani, D. Capper, S. Schmid, D. Kaul, Diffuse paediatric-type high-grade glioma, H3-wildtype and IDH-wildtype: case series of a new entity, Brain Tumor Pathol, 40 (2023) 204-214.

Figure legends

Fig. 1 Molecular landscape of the cGBM cohort

a Schematic workflow of the current study.

b LTS and STS samples matched to the established DNA methylation class.

c Clinical and molecular characteristics of the entire 72-patient cGBM cohort. Each column represents a patient, ordered by the number of somatic variants across the entire genome. Red asterisk (*) indicates no data available.

d-e Contribution of COSMIC signatures in LTS (**d**) and STS (**e**).

Fig. 2 Genomic alteration landscape of LTS and STS

a-d Dot plot comparing TMB (**a**), MATH score (**b**), gene fusion (**c**) and CNV (**d**) between LTS and STS patients.

e Genome regions with CN gain (left) and loss (right), respectively.

f Bar plot showing top significantly different genomic alterations between LTS and STS.

Fig. 3 Transcriptomic difference and tumor microenvironment of LTS and STS

a Volcano plot showing gene expression variation between LTS and STS patients.

b GO analysis of 2098 differentially expressed genes. The olfactory-related pathways are highly enriched.

c Stacked bar plot showing the infiltration proportion of immune cells.

d Heatmap showing hierarchical clustering of immune cell infiltration significantly different between LTS and STS.

e Representative images (up) and quantification (down) of immune cell marker IHC in GBM patients.

Fig. 4 DNA methylation pattern of LTS and STS

a Boxplot showing methylation of different CpG gene loci (left) and CpG types (right).

b Volcano plot showing normalized beta value of DMP.

c Dot plot showing KEGG pathways enriched in DMP.

d Venn diagram showing overlap between clusters R2 and M2 genes (up), and patients marked by clusters R2 and M2 (down).

Fig. 5 Molecular profiling of m-GBM and pedHGG

a-d Dot plot comparing TMB (**a**), MATH score (**b**), gene fusion (**c**) and CNV (**d**) between LTS m-GBM and STS m-GBM patients.

e Bar plot showing top significantly different genomic alterations between LTS m-GBM and STS m-GBM patients.

f GO analysis of 1540 differentially expressed genes. The olfactory-related pathways are highly enriched.

g Boxplot showing methylation of different CpG types in LTS m-GBM and STS m-GBM patients.

h Overall survival for STS m-GBM and pedHGG.

i Representative hematoxylin and eosin staining of one STS m-GBM and one pedHGG.

j Copy number alteration plot of representative LTS m-GBM, STS m-GBM and pedHGG cases.

k Boxplot showing methylation of different CpG types in STS m-GBM and pedHGG.

Fig. 6 LTS-specific features

a-e LASSO regression patterns showing correlation between performance and the size of input features. The blue curve, corresponding to the left Y axis, shows the prediction accuracy. The red curve, corresponding to the right Y axis, shows the number of non-zero weighted features. The green dashed line shows the optimal C value chosen for the current model to maximize prediction accuracy and minimize the size of input features. The input features were clinical character (**a**), SNV (**b**), RNA expression (**c**), methylation status (**d**) and multi-omics data (**e**), respectively.

f Heatmap showing hierarchical clustering based on multi-omics data as in (**e**).

Supplementary Fig. 1 Patient selection, SNV, CNV and gene fusion of the cGBM cohort

a Patient selection flowchart for LTS (left) and STS (right).

b t-SNE analysis of DNA methylation profiles for LTS and STS.

c-d Oncoplot showing SNV of the cGBM cohort (**c**), and comparison between LTS and STS (**d**). Genes are presented in descending order by the mutation rate.

e-f Oncoplot showing most frequent somatic CNV of the cGBM cohort (**e**) and comparison between LTS and STS (**f**).

g Oncoplot of gene fusions presented in descending order.

h Oncoplot of SNV in TCGA-GBM (left) and cGBM (right) cohorts.

Supplementary Fig. 2 Comparison of genomic alteration between LTS and STS

a Forest plot of SNV with top statistical significance.

b-c Lollipop plot of *CASC5* (**b**) and *SPEN* (**c**) mutations. Y axis represents mutation frequency and X axis represents the sequence change at protein level.

d Forest plot of CNV with top statistical significance.

Supplementary Fig. 3 Transcriptomic difference between LTS and STS

a Heatmap of top 5000 differentially expressed genes.

b KEGG pathway analysis of DEG.

Supplementary Fig. 4 Tumor microenvironment of LTS and STS

Boxplot comparing immune cell infiltration between LTS and STS.

Supplementary Fig. 5 DNA methylation pattern of LTS and STS

a Distribution of methylation beta value in LTS and STS.

b Genome distribution of DMP in different CpG gene loci (left) and CpG types (right).

c PCA of DMP normalized beta value.

d Heatmap showing hierarchical clustering of DMP based on normalized beta value.

e-f Boxplot showing methylation of different CpG gene loci in LTS m-GBM and STS m-GBM (**e**), and in pedHGG and STS m-GBM (**f**).

Supplementary Fig. 6 LTS-specific features and molecular characteristics of LTS in publicly available dataset

a LASSO regression patterns showing correlation between performance and GBM biomarkers.

b-c Heatmaps showing hierarchical clustering based on RNA expression as in **Fig. 6c** (**b**) and methylation status as in **Fig. 6d** (**c**).

d GO analysis of genes involved in the multi-omics data as in **Fig. 6e**.

e Oncoplot showing somatic SNV in descending order by frequency in publicly available dataset.

f GO analysis of differentially expressed genes between LTS and STS in publicly available dataset.

g-h Boxplot comparing methylation of different CpG gene loci (**g**) and CpG types (**h**) between LTS and STS.

Table 1 Methylation class of LTS and STS cohorts

Methylation class	LTS	STS	P value
Glioblastoma, IDH-wildtype	8(22.9%)	9(24.3%)	>0.999
Glioblastoma, IDH-wildtype, mesenchymal subtype	7(20.0%)	7(18.9%)	>0.999
Glioblastoma, IDH-wildtype, RTK2 subtype	5(14.2%)	7(18.9%)	0.754
Glioblastoma, IDH-wildtype, RTK1 subtype	1(2.9%)	4(10.9%)	0.358
Glioblastoma, IDH-wildtype, mesenchymal subtype, subclass B	1(2.9%)	0	0.486
Glioblastoma, IDH-wildtype with primitive neuronal component	1(2.9%)	1(2.7%)	>0.999
Adult-type diffuse high grade glioma, IDH-wildtype, subtype E	1(2.9%)	0	0.486
Adult-type diffuse high grade glioma, IDH-wildtype, subtype F	0	1(2.7%)	>0.999
Pleomorphic xanthoastrocytoma	2(5.7%)	0	0.233
CNS tumor with BCOR/BCORL1 fusion	1(2.9%)	0	0.486
Diffuse pediatric-type high grade glioma, RTK1 subtype, subclass A	0	3(8.1%)	0.240
diffuse pediatric-type high grade glioma, H3 wildtype and IDH wild type, Subtype A	0	1(2.7%)	>0.999
Inflammatory microenvironment	3(8.5%)	3(8.1%)	>0.999
No match (score < 0.9)	5(14.2%)	1(2.7%)	0.102

Table 2 Clinicopathological characteristics of LTS and STS patients

Characteristic	All (n = 72)	LTS (n = 35)	STS (n = 37)	P value
Gender				0.459
Female	25	14	11	
Male	47	21	26	
Age, year				>0.999
< 55	36	17	19	
≥ 55	36	18	18	
***MGMT* promoter methylation**				0.351
Yes	41	22	19	
No	31	13	18	
***TERT* promoter mutation**				0.797
Yes	51	24	27	
No	21	11	10	
***EGFR* amplification**				0.817
Yes	32	15	17	
No	40	20	20	
+7/-10 signature				>0.999
Yes	36	17	19	
No	36	18	18	
***ATRX* mutation**				>0.999
Yes	7	3	4	
No	65	32	33	
***BRAF* mutation**				0.609
Yes	3	2	1	
No	69	33	36	
Location				0.884
Frontal	16	7	9	
Temporal	20	10	10	
Parietal	9	5	4	
Occipital	5	2	3	
Other	4	3	1	
multiple lobes	18	8	10	
Dominant hemisphere				0.101
Dominant	38	18	20	
Nondominant	30	13	17	
Bilateral	4	4	0	
Surgery				0.358
Total resection	49	25	24	
Subtotal resection	7	3	4	
Unknown	16	7	9	
Treatment				0.186
TMZ+RT	59	29	30	
TMZ	3	0	3	
Unknown	10	6	4	

Figure 1

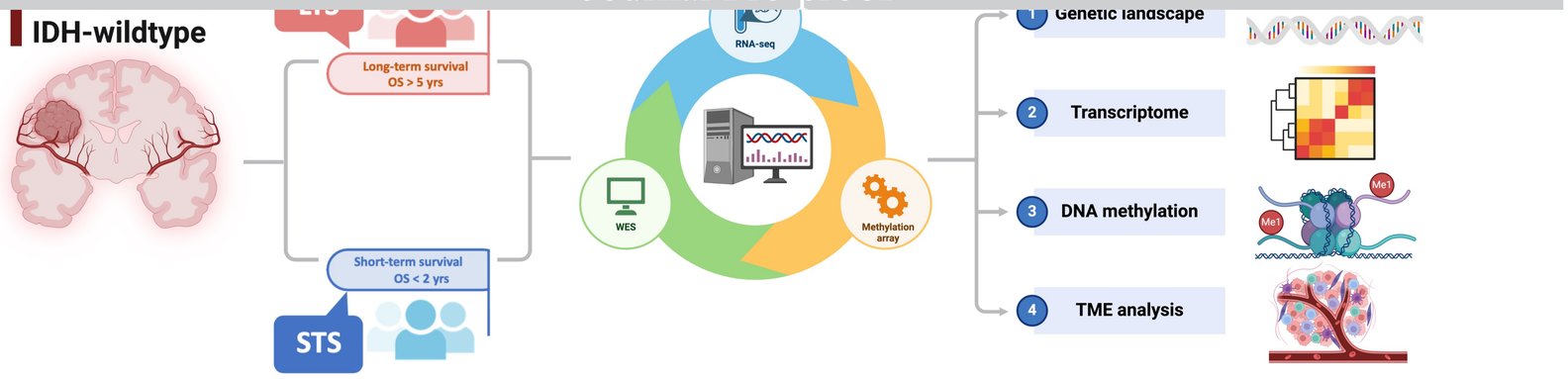

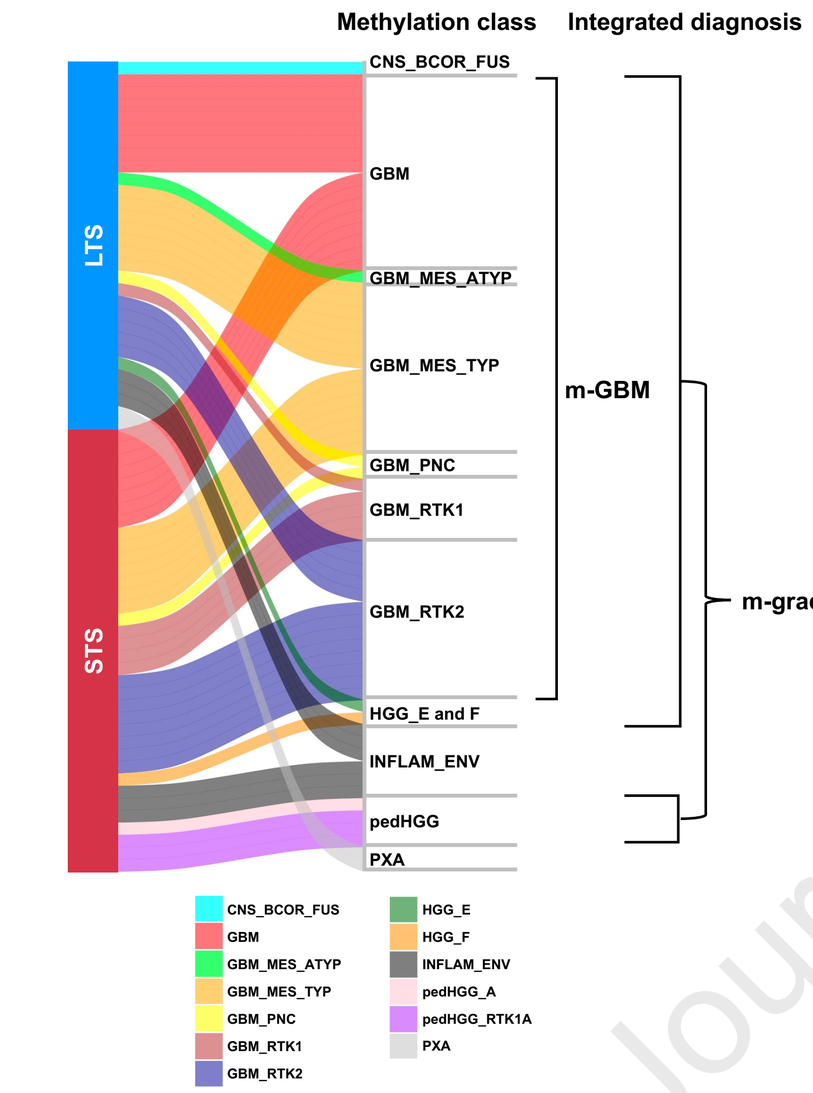

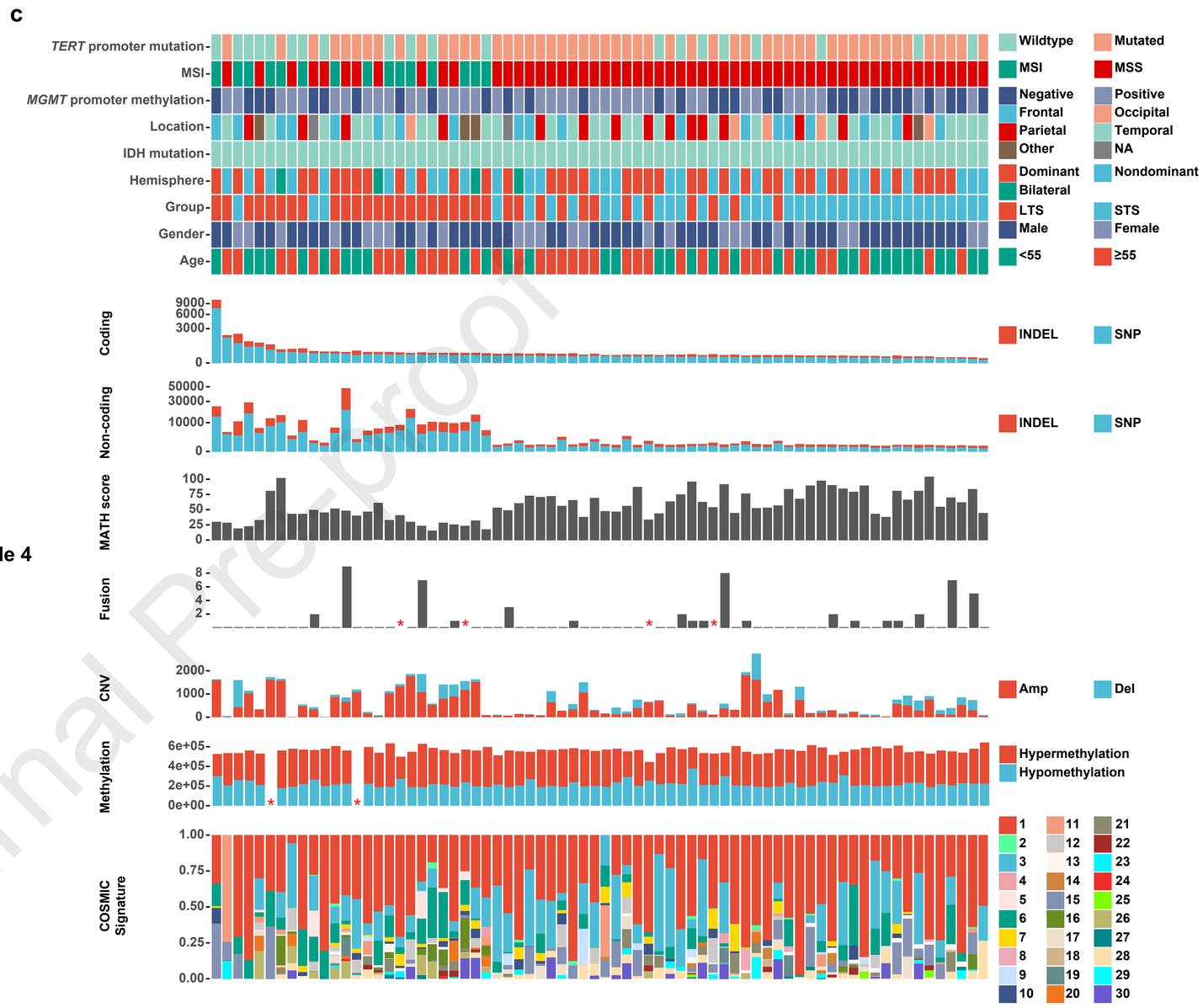

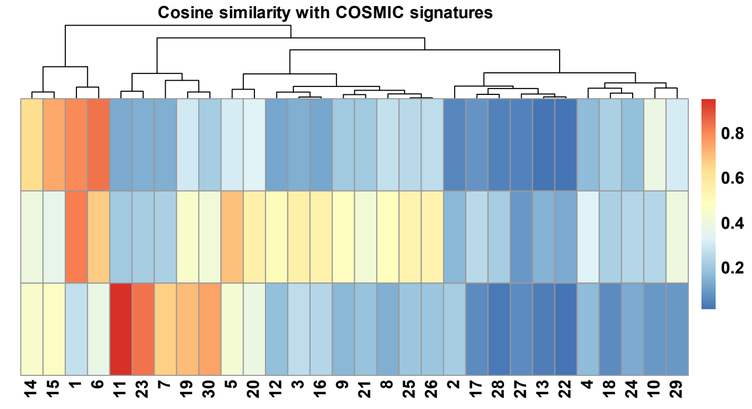

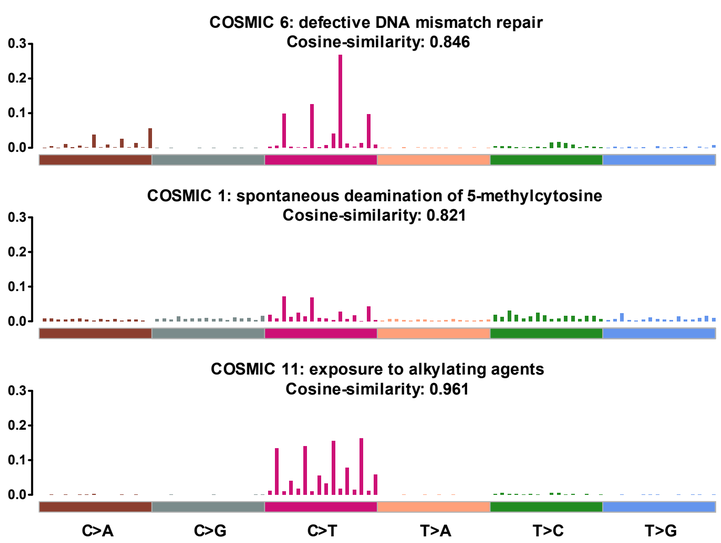

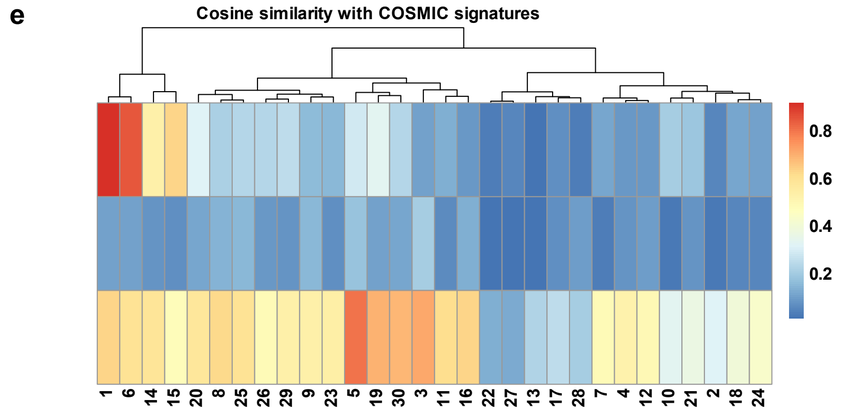

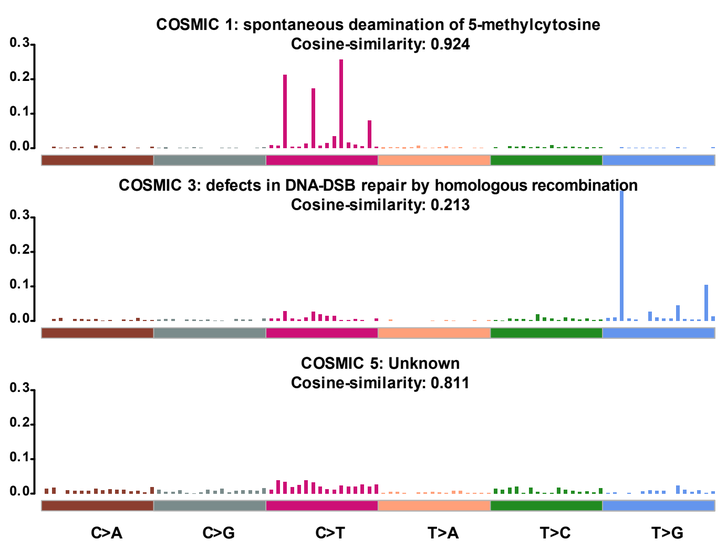

Figure 2

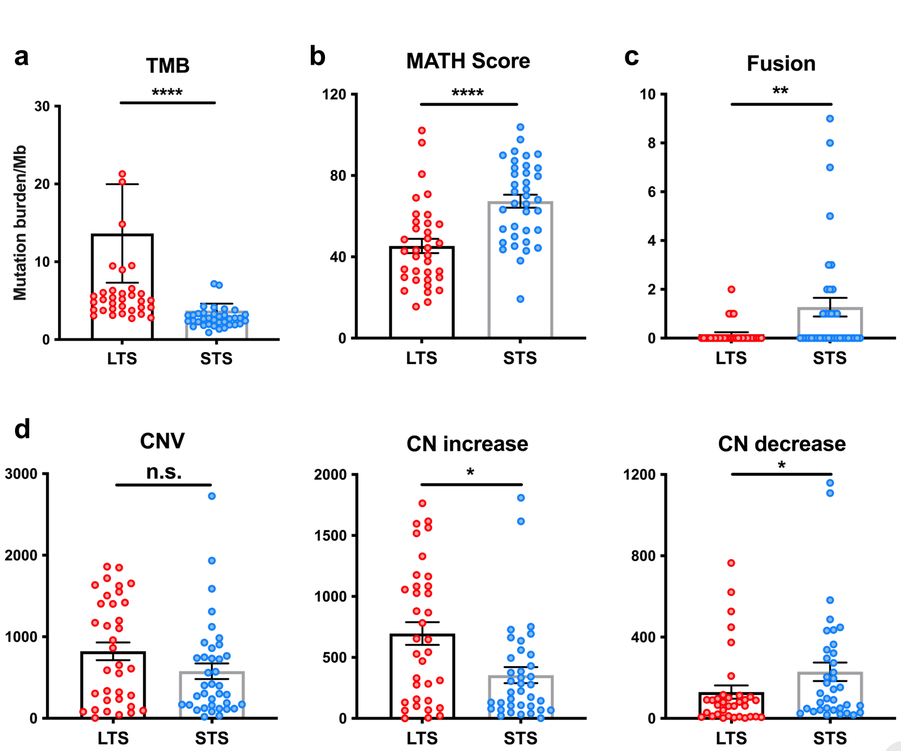

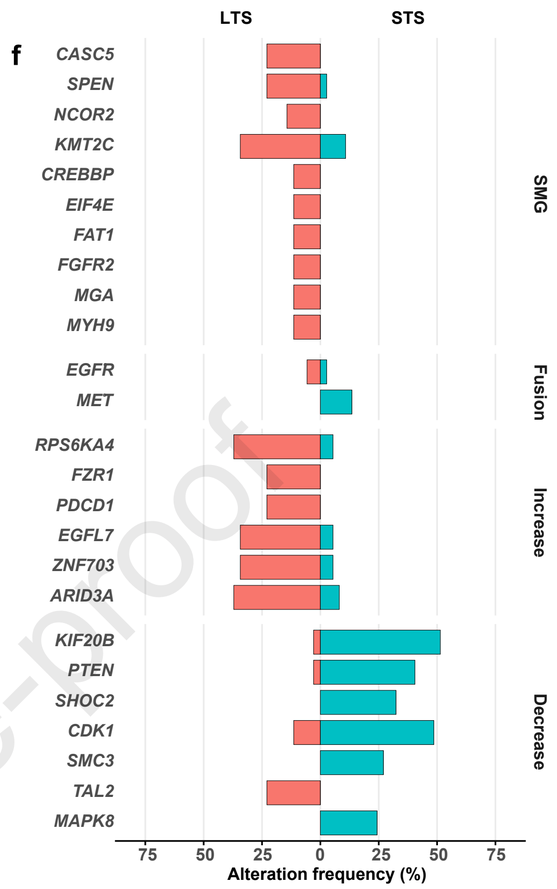

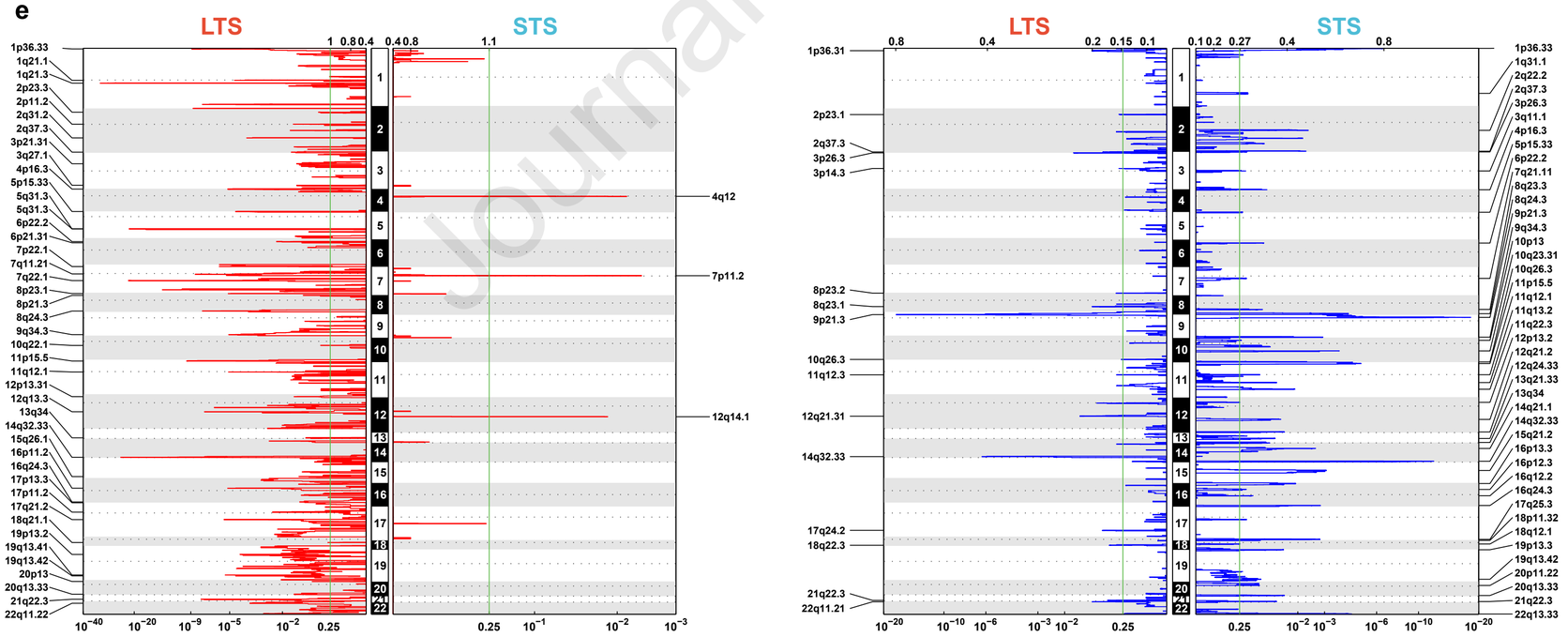

Figure 3

a

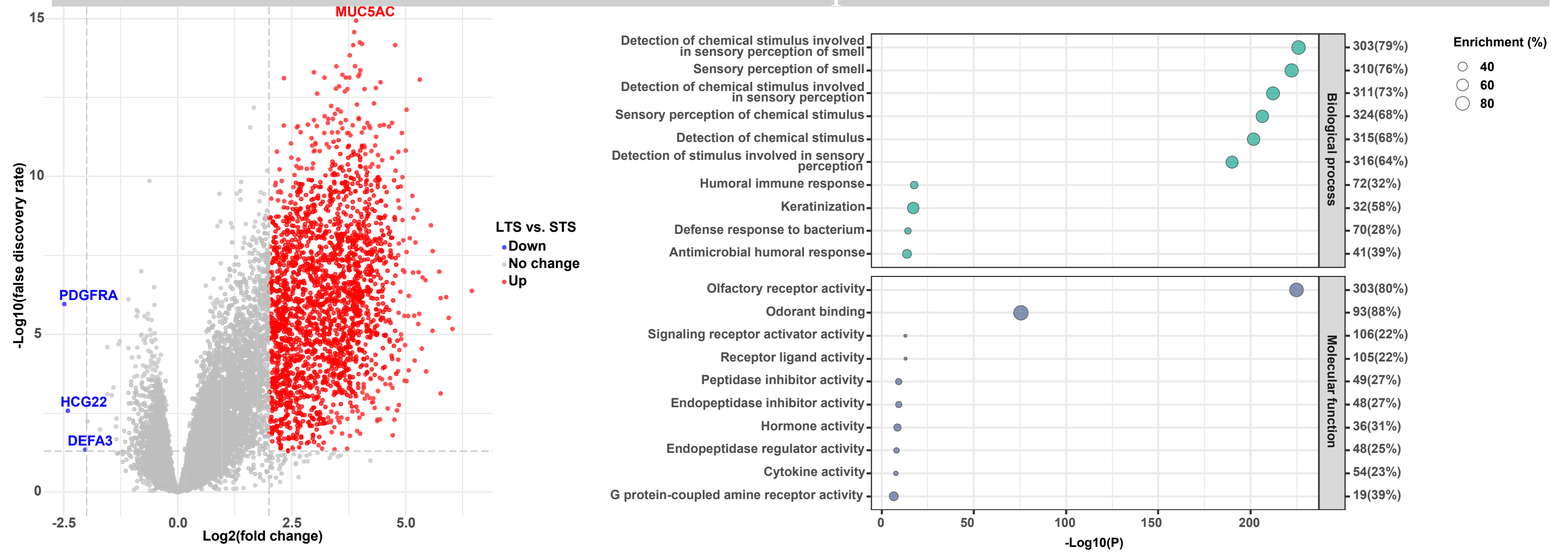

c

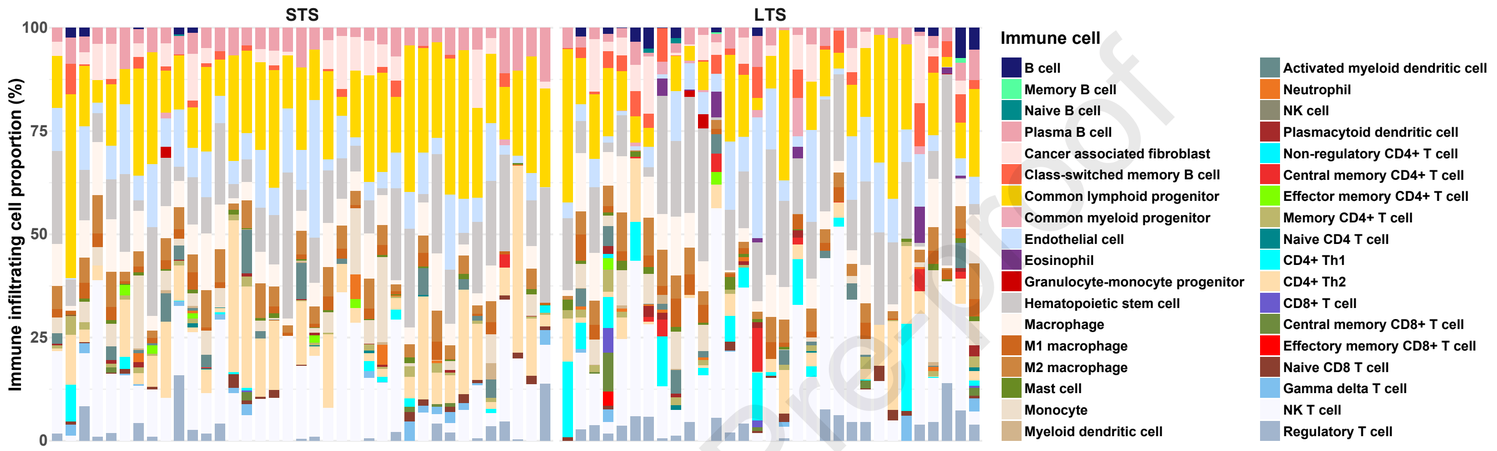

d

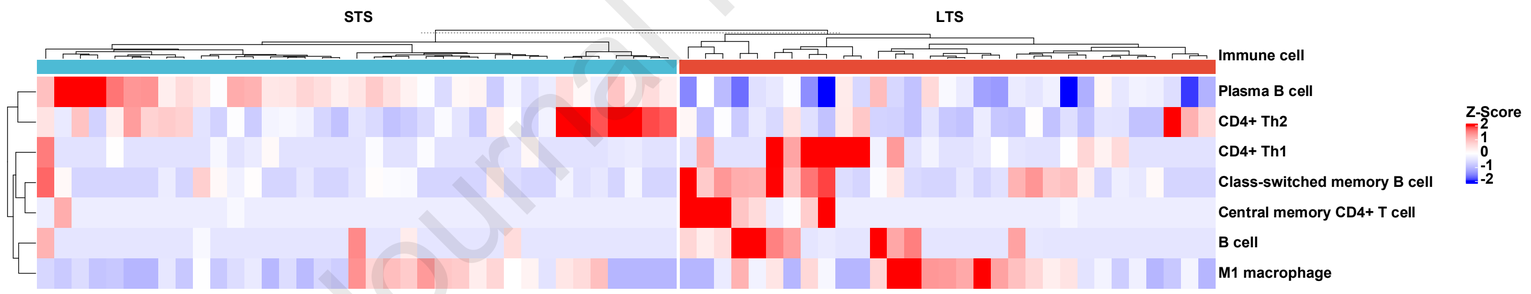

e

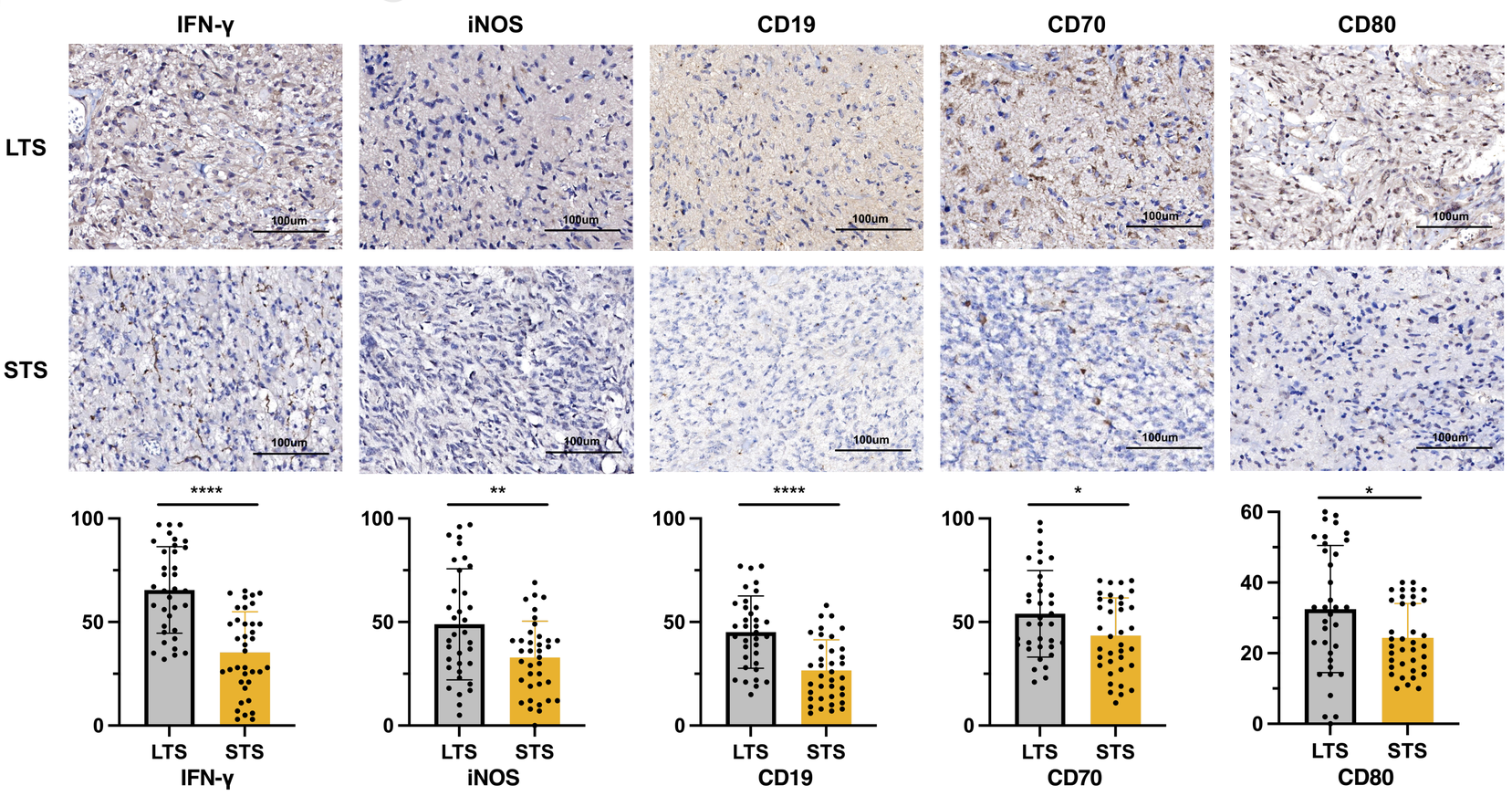

Figure 4

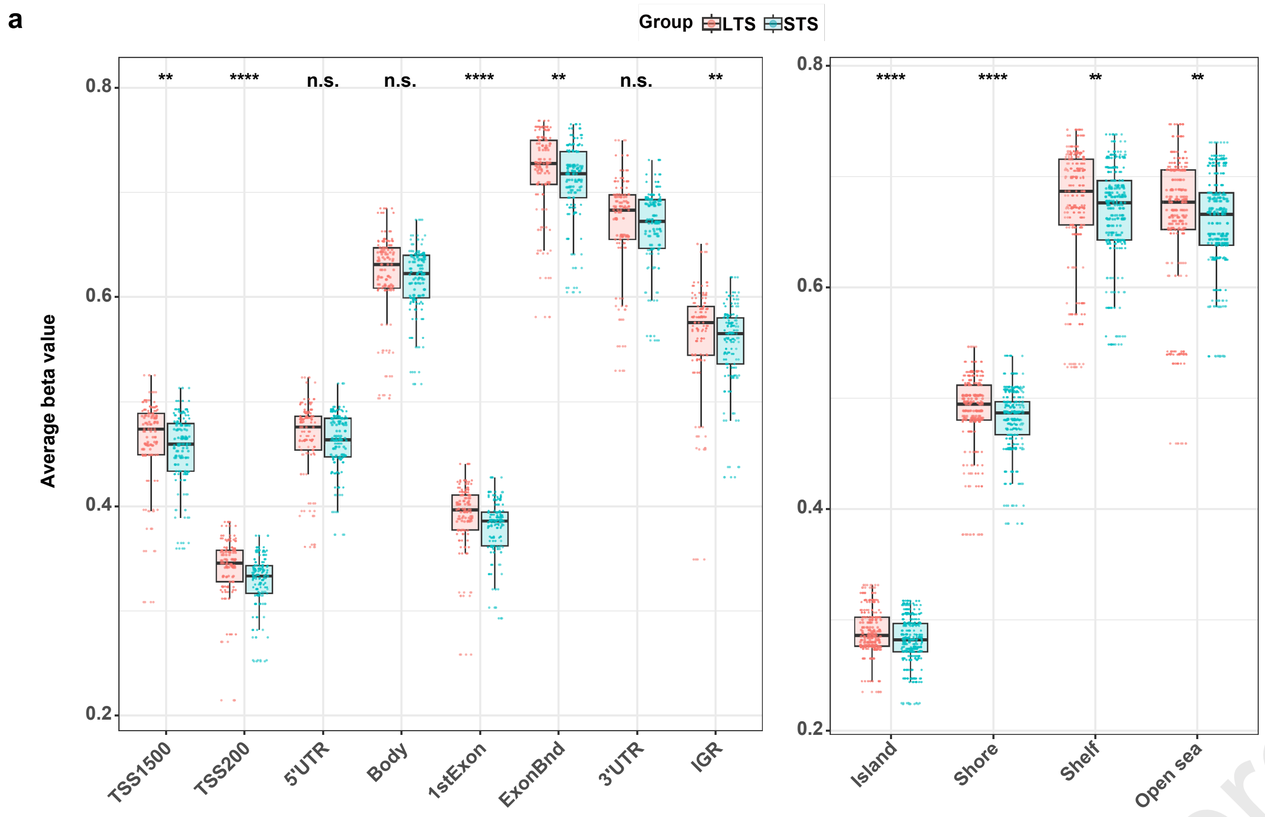

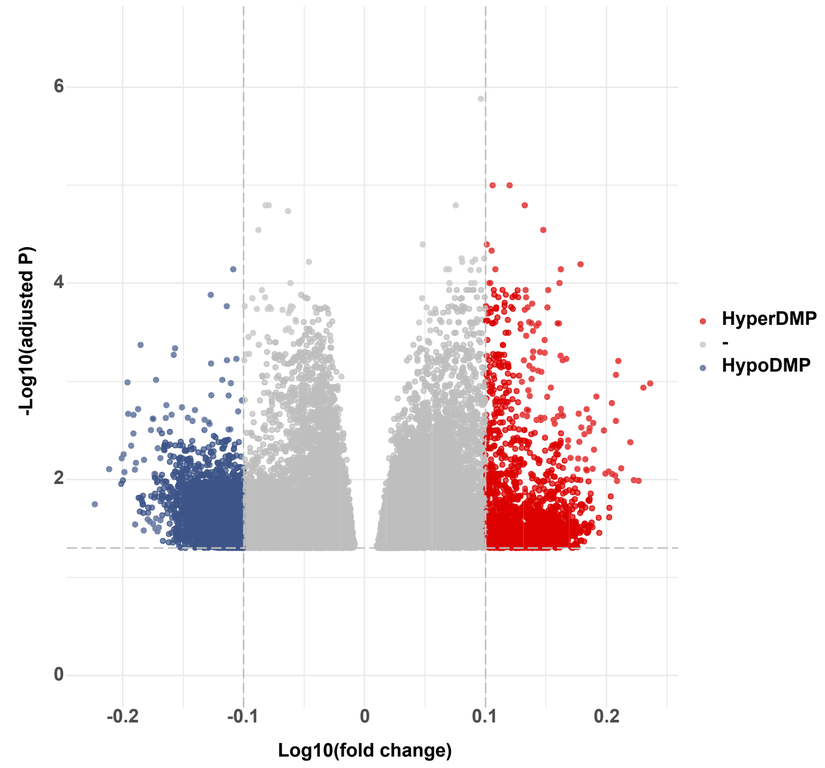

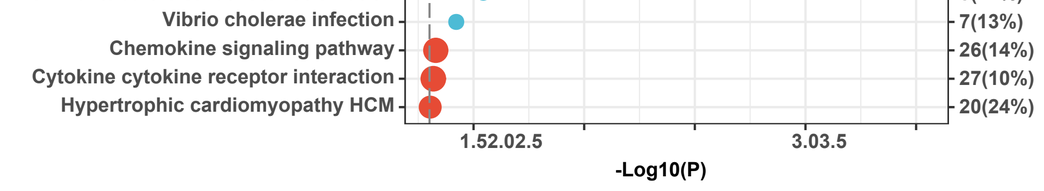

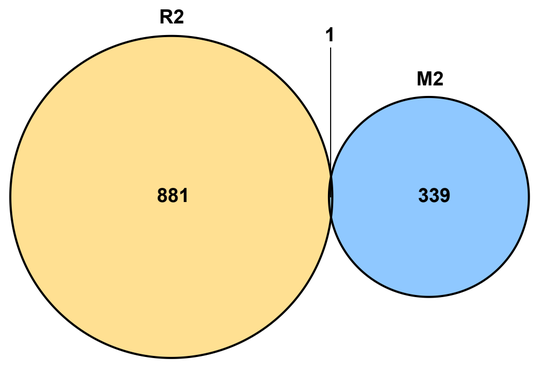

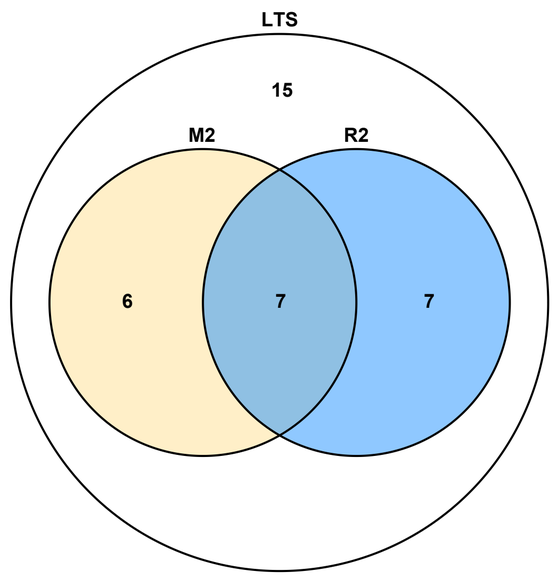

Figure 6

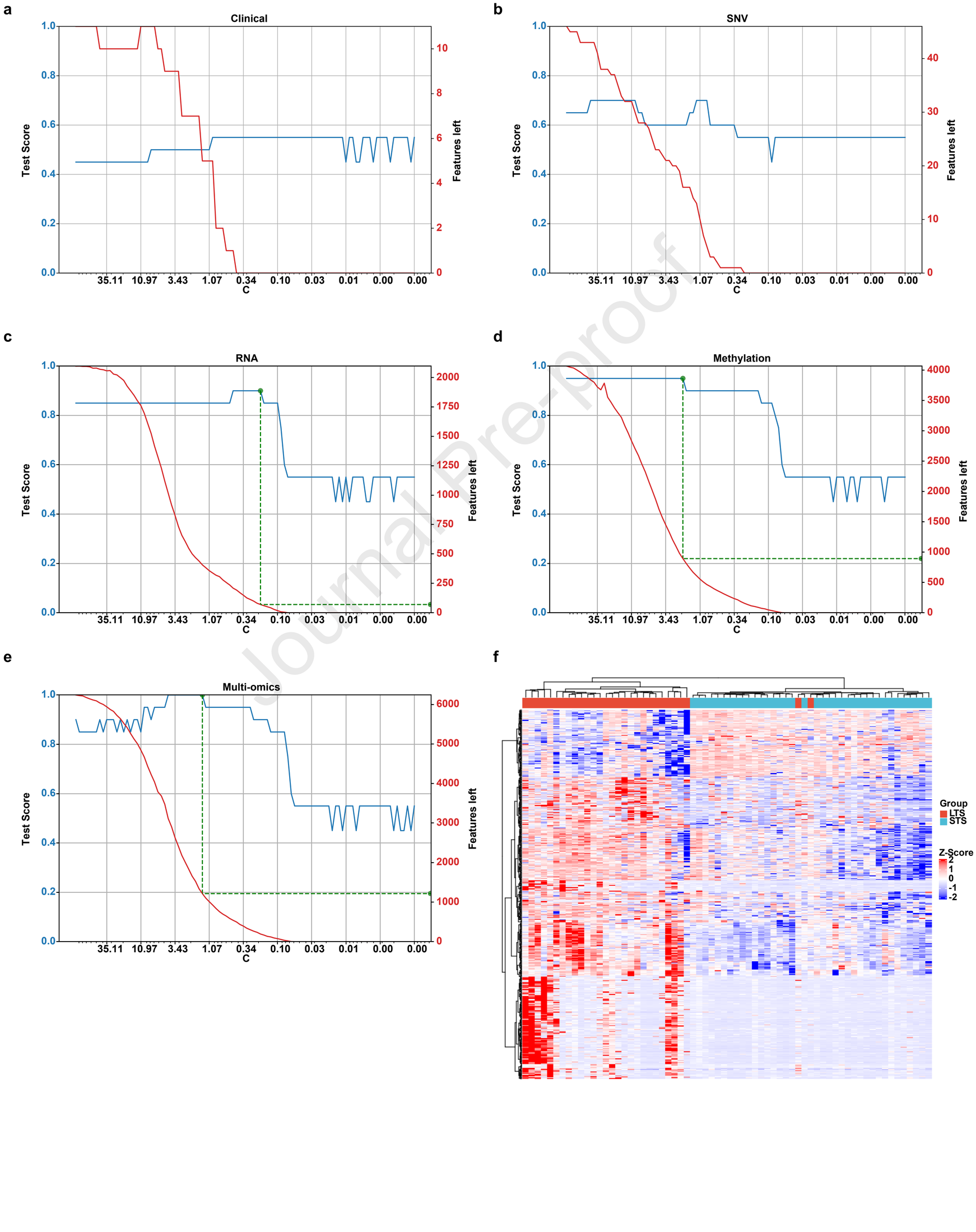

Figure 5

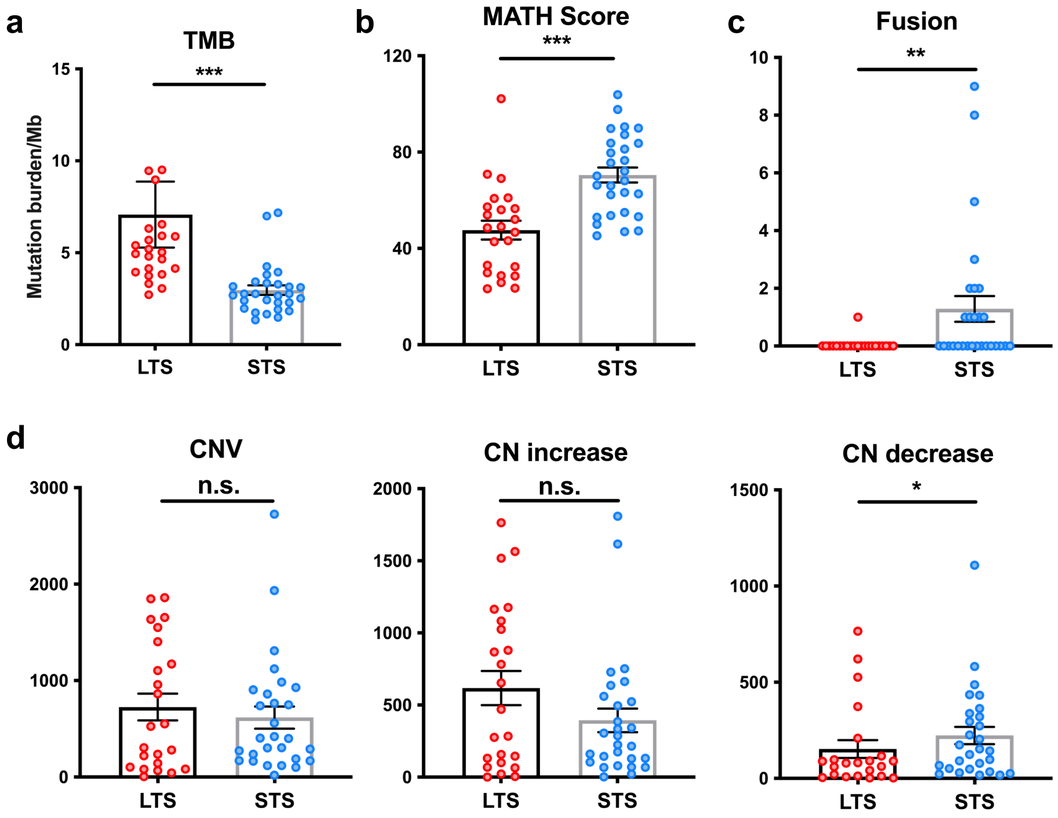

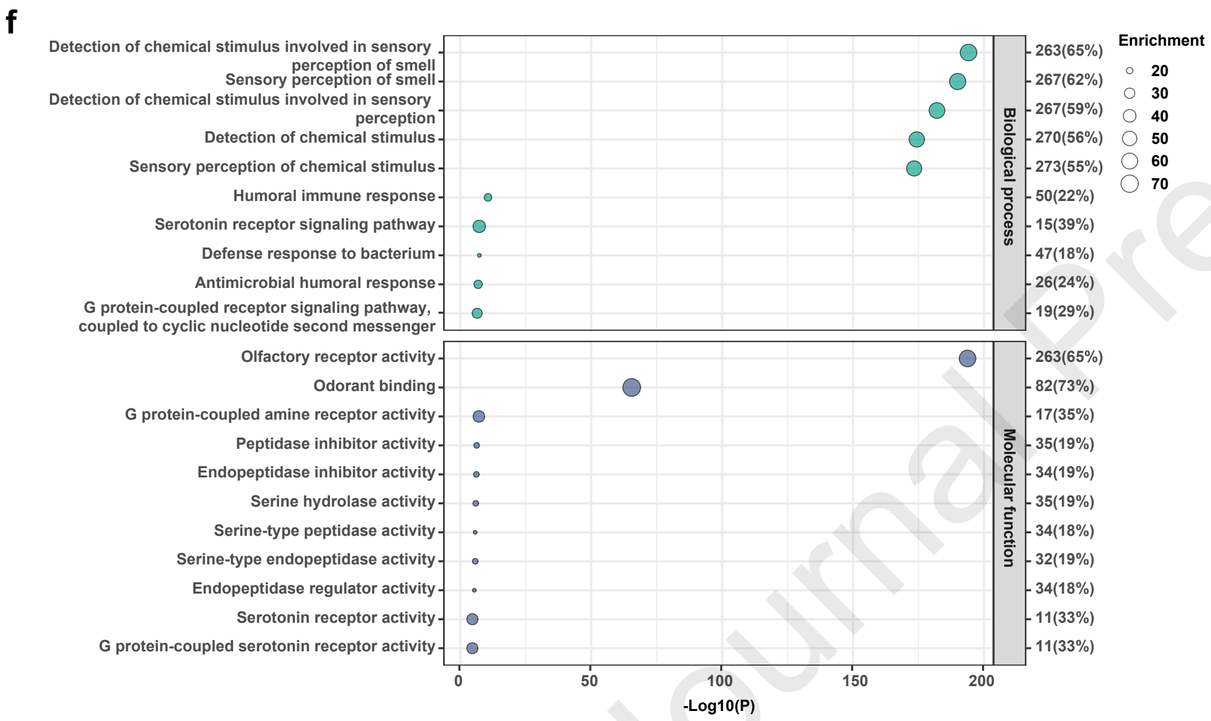

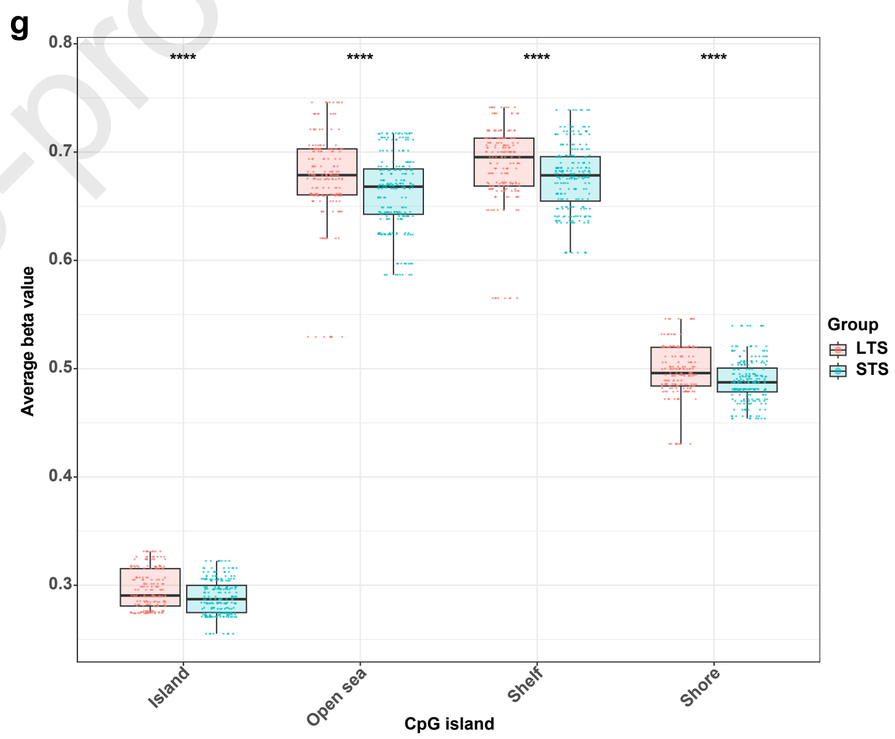

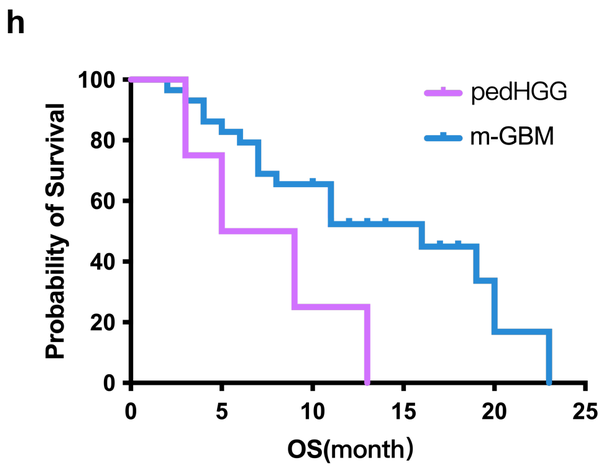

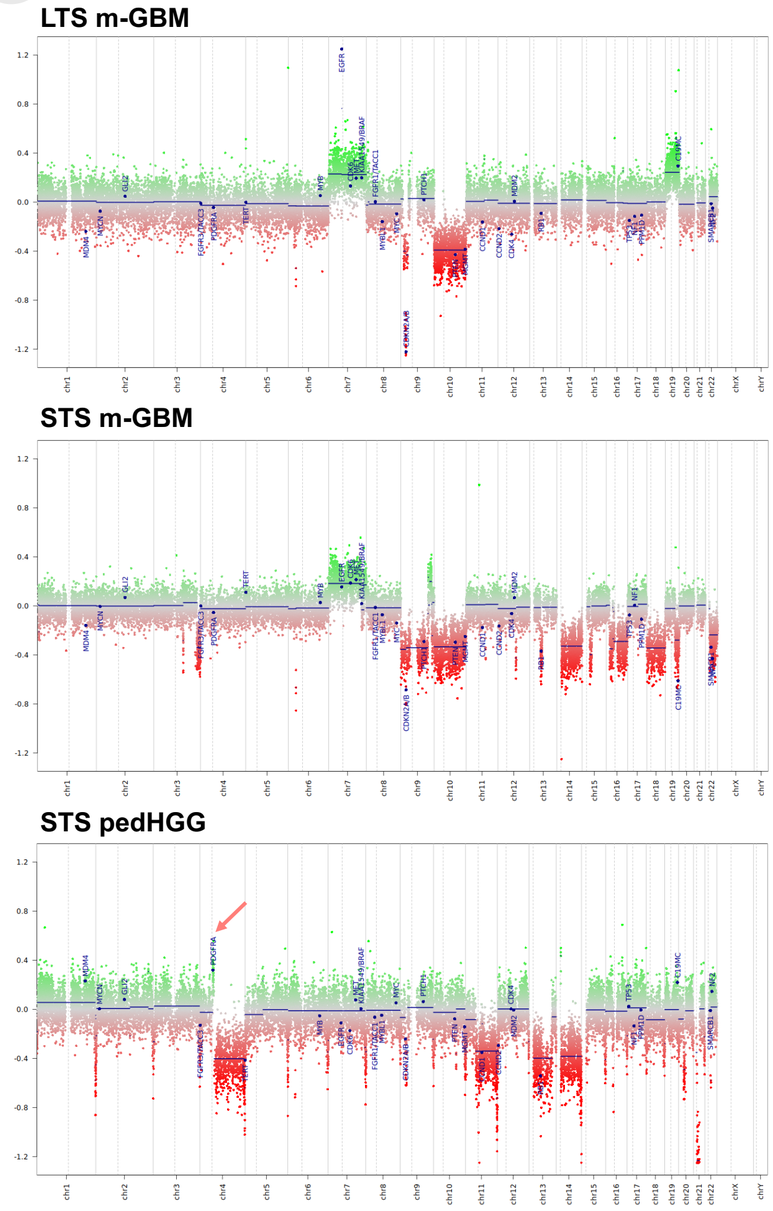

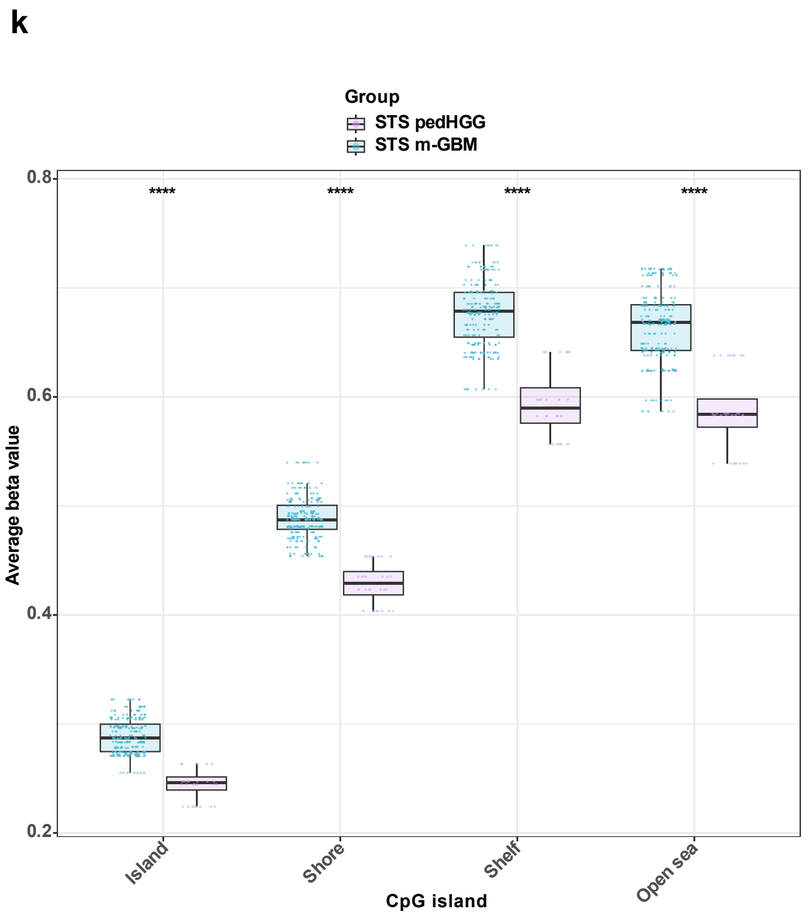

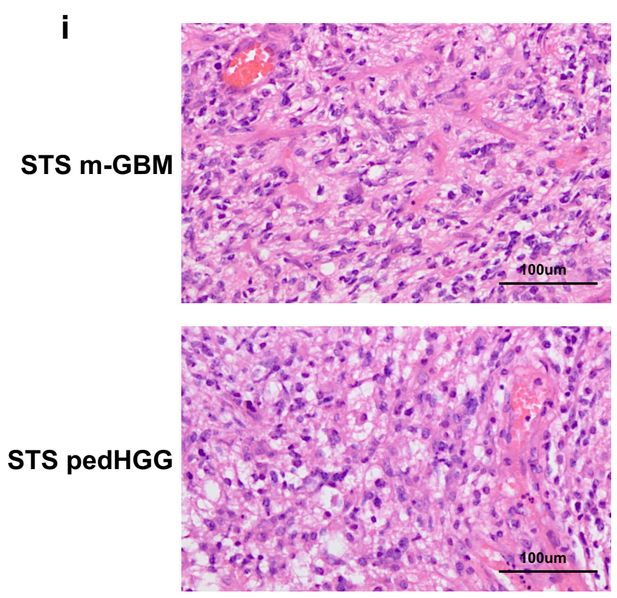

LTS were characterized by hypermethylated genome, copy number increase and higher TMB

LTS demonstrated distinct TME and olfactory transduction-related pathway enrichment

STS showed heterogeneous tumor tissue, more gene fusion and copy number decrease

Most LTS and STS were confirmed as methylation class-defined GBM (m-GBM)

The molecular features of m-GBM patients were in accordance with the entire cohort

Declaration of interests

☒ The authors declare that they have no known competing financial interests or personal relationships that could have appeared to influence the work reported in this paper.

☐The authors declare the following financial interests/personal relationships which may be considered as potential competing interests: